pubs.acs.org/Biomac

Article

Injectable Slow-Release Hydrogel Formulation of a Plant Virus-Based COVID-19 Vaccine Candidate

Christian Isalomboto Nkanga, Oscar A. Ortega-Rivera, Matthew D. Shin, Miguel A. Moreno-Gonzalez, and Nicole F. Steinmetz*

Cite This: *Biomacromolecules* 2022, 23, 1812−1825

Read Online

ACCESS | Metrics & More | Article Recommendations | Supporting Information

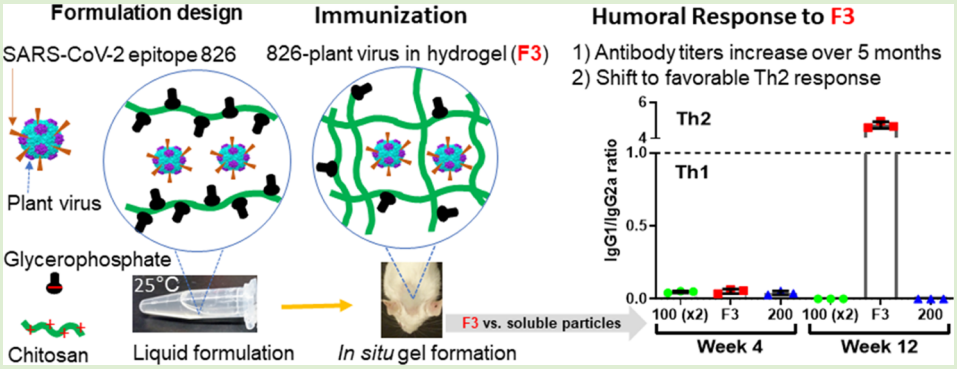

ABSTRACT: Cowpea mosaic virus (CPMV) is a potent immunogenic adjuvant and epitope display platform for the development of vaccines against cancers and infectious diseases, including coronavirus disease 2019. However, the proteinaceous CPMV nanoparticles are rapidly degraded in vivo. Multiple doses are therefore required to ensure long-lasting immunity, which is not ideal for global mass vaccination campaigns. Therefore, we formulated CPMV nanoparticles in injectable hydrogels to achieve slow particle release and prolonged immunostimulation. Liquid formulations were prepared from chitosan and glycerophosphate (GP) before homogenization with CPMV particles at room temperature. The formulations containing high-molecular-weight chitosan and 0−4.5 mg mL^{-1} CPMV gelled rapidly at 37 °C (5−8 min) and slowly released cyanine 5-CPMV particles in vitro and in vivo. Importantly, when a hydrogel containing CPMV displaying severe acute respiratory syndrome coronavirus 2 spike protein epitope 826 (amino acid 809−826) was administered to mice as a single subcutaneous injection, it elicited an antibody response that was sustained over 20 weeks, with an associated shift from Th1 to Th2 bias. Antibody titers were improved at later time points (weeks 16 and 20) comparing the hydrogel versus soluble vaccine candidates; furthermore, the soluble vaccine candidates retained Th1 bias. We conclude that CPMV nanoparticles can be formulated effectively in chitosan/GP hydrogels and are released as intact particles for several months with conserved immunotherapeutic efficacy. The injectable hydrogel containing epitope-labeled CPMV offers a promising single-dose vaccine platform for the prevention of future pandemics as well as a strategy to develop long-lasting plant virus-based nanomedicines.

INTRODUCTION

The pandemic of coronavirus disease 2019 (COVID-19) is an unprecedented global public health challenge due to the transmissibility, morbidity, and mortality associated with severe acute respiratory syndrome coronavirus 2 (SARS-CoV-2). There were more than 83 million positive cases and 3 million deaths in the first year following the initial outbreak in December 2019.[1−3] Several multidose vaccines were rapidly developed and approved, including the Pfizer-BioNTech BNT162b2,[4] Oxford-AstraZeneca,[5] and Moderna vaccines.[6] However, despite global mass vaccination campaigns beginning in December 2020, the number of positive cases had risen to more than 281 million by the end of 2021, with ∼5 million deaths.[7] These data indicate that global morbidity increased 2.4-fold during the vaccination period,[3] whereas the mortality rate decreased.[7] In part, these figures represent the contrast between the exponential spread of the virus and the logistical and supply-chain issues facing the distribution of vaccines,[8] including the requirement for cold chain continuity for some of the products[9] and the choice between prioritizing first dose coverage and the completion of two-dose schedules according

Received: January 24, 2022
Revised: March 9, 2022
Published: March 28, 2022

https://doi.org/10.1021/acs.biomac.2c00112
Biomacromolecules 2022, 23, 1812−1825

to clinical guidelines.[10−13] In this context, a long-acting single-dose vaccine would be an ideal alternative, providing wider coverage while ensuring complete protection by eliciting sustained immunological responses.

During the pandemic, the emergence of more contagious SARS-CoV-2 variants[14−17] that can overcome prior immunity[18] has highlighted the potential for reinfection and loss of vaccine efficacy.[19] This can be addressed by updating vaccines to maintain protection,[20,21] but an alternative solution is the development of vaccines that elicit broadly neutralizing antibodies. At the end of 2021, there were 23 COVID-19 vaccines already approved for emergency use in humans and 329 vaccine candidates undergoing clinical (111) or preclinical (218) tests.[22] These represented a range of conventional and novel vaccine platforms including inactivated whole viruses (e.g., CoronaVac and Covaxin), mRNA-loaded liposomes (e.g., BNT162b2 and mRNA-1273), adenovirus vectors (e.g., ChAdOx1 nCoV-19, CTII-nCoV, and Sputnik V), and virus-like particles (e.g., NVX-CoV2373).[23] These vaccines elicit a neutralizing antibody response against the SARS-CoV-2 spike (S) protein and achieved 65−96% protective efficacy against morbidity and mortality in phase 3 trials.[4,5,24−28] The vaccines are effective because the S protein protrudes from the virus surface and is recognized by angiotensin-converting enzyme 2 on the host cell surface, which facilitates the uptake of viral particles.[29] However, the efficacy of vaccines targeting the S protein declines due to the rapid evolution of variants that accumulate mutations.[30−33] Mutations occur in the N-terminal domain, including L18F, D80A, D215G, and Δ242-244; the receptor-binding domain (RBD), including K417N, E484K, and N501Y; and other regions that maintain spike stability and functionality, including D614G and P681R.[34−37] It may be more appropriate to select broadly conserved epitopes for the development of vaccines rather than using the entire S protein.

The RBD is the binding site for most neutralizing antibodies against SARS-CoV-2.[38] We recently demonstrated that three B-cell epitopes (peptide sequences 553−570, 625−636, and 809−826), which are common to many SARS-CoV-2 variants, are suitable for the development of effective pan-specific vaccines against SARS-CoV-2.[39] To enhance the immune response, these peptide epitopes were attached to cowpea mosaic virus (CPMV) or virus-like particles derived from bacteriophage Qβ, which function as a combined adjuvant and epitope nanocarrier, promoting trafficking across draining lymph nodes and interactions with antigen-presenting cells.[40,41] CPMV has a bipartite RNA genome encapsulated in a 30 nm icosahedral capsid consisting of 60 asymmetrical copies of small (24 kDa) and large (41 kDa) coat protein (CP) subunits.[42] Both the capsid and RNA are immunostimulatory, therefore rendering CPMV a potent adjuvant. For example, the strong immunogenicity of native CPMV[44,45] makes it an effective in situ vaccine against various tumors in mouse models[41,46,47] and canine patients.[48] It also serves as a delivery platform and multiple copies of the SARS-CoV-2 peptide epitopes can be displayed via chemical bioconjugation.[43] When tested as soluble prime-boost formulations, microneedle patches, or slow-release poly(lactic-*co*-glycolic acid) (PLGA) implants, the CPMV- and Qβ-based COVID-19 vaccine candidate formulations elicited neutralizing antibodies against SARS-CoV-2, and the soluble prime-boost vaccine (CPMV conjugated to the epitope sequence 809−826) elicited a neutralization titer comparable to Moderna's mRNA-1273 vaccine.[39] The Qβ formulation maintained efficacy when formulated as a PLGA implant, but in a previous study with a similar approach against SARS-CoV, the efficacy of CPMV-based vaccines declined significantly in this format when administered as a single dose.[43] This reflected the lower immunostimulatory response caused by the loss of CPMV RNA during freeze-drying, as required for implant formulation.[49] The efficacy of a CPMV-based vaccine displaying the 809−826 epitope sequence (826-CPMV) could perhaps be improved by investigating alternative single-dose formulations, such as those based on the natural biopolymer chitosan.

Chitosan is a polysaccharide produced by the deacetylation of chitin.[57] It is generally regarded as safe as an excipient and is therefore considered to be biocompatible, nonimmunogenic, and biodegradable.[50,51] It is already approved for products such as BST-CarGel for the regeneration of cartilage.[52] Many studies have reported excellent immune-enhancing capability of chitosan as a vaccine adjuvant for nasal,[53] parenteral,[54] and subcutaneous administrations.[55] Chitosan-based hydrogels are produced by mixing chitosan with β-glycerophosphate (GP) to yield liquid formulations that are fluid at room temperature but form a gel at body temperature. This thermo-responsive behavior is driven by the interactions between GP and the polar backbone of chitosan, which prevents polymer precipitation, balances the pH, and triggers gelation when heated.[56−58] Such thermo-responsive hydrogels are advantageous because they are simple to prepare and inject.[59,60] Chitosan/GP hydrogels have been extensively used for drug delivery,[61,62] tissue regeneration/repair,[63,64] and the slow release of nanoparticles.[65,66]

Here, we report the development of an in situ forming chitosan/GP hydrogel loaded with 826-CPMV as a single-dose vaccine against COVID-19. We initially prepared chitosan/GP hydrogels containing native CPMV particles for formulation design and optimization before testing CPMV labeled with the fluorophore sulfo-cyanine 5 (Cy5) as a cargo model for the characterization of in vitro/in vivo release profiles by fluorescence analysis. We then prepared 826-CPMV particles formulated as chitosan/GP hydrogels and immunized BALB/c mice subcutaneously. We monitored the antibody response for 20 weeks, comparing the hydrogel to soluble formulations in terms of antibody titers and subtypes.

EXPERIMENTAL SECTION

Preparation of CPMV Nanoparticles. *Preparation of Native CPMV.* CMPV was propagated in and extracted from the leaves of black-eyed pea plants (*Vigna unguiculata*) as previously described.[67,68] The frozen leaf tissue (100 g) was homogenized in 300 mL of 0.1 M potassium phosphate (KP) buffer (pH 7.0) and then filtered and centrifuged (18 500*g*, 20 min, 4 °C) to remove plant debris. The supernatant was extracted with 1:1 chloroform:1-butanol, and the aqueous phase was mixed with 0.2 M NaCl and 8% PEG 8000 for CPMV precipitation. The mixture was centrifuged (30 000*g*, 15 min, 4 °C), and the pellet was resuspended in 0.01 M KP buffer. After a further round of centrifugation (13 500*g*, 15 min, 4 °C) to remove aggregates, the supernatant was purified on a 10−40% sucrose gradient. The bright bands were isolated and purified by ultracentrifugation (42 000 rpm, 2.5 h, 4 °C) using an Optima L-90K centrifuge with rotor type 50.2 Ti (Beckman Coulter, Brea, CA, USA). CPMV particles were dispersed in 0.1 M KP buffer, and the CP concentration was determined using a NanoDrop 2000 UV/visible spectrophotometer (Thermo Fisher Scientific, Waltham, MA, USA) at 260 nm using a molar extinction coefficient ($\varepsilon_{260\ nm}$) of 8.1 mg^{-1} mL cm^{-1}.

Conjugation of CPMV to Sulfo-Cy5. We prepared Cy5-CPMV particles by conjugating CPMV lysine residues to the *N*-

https://doi.org/10.1021/acs.biomac.2c00112
Biomacromolecules 2022, 23, 1812−1825

hydroxysuccinimide (NHS)-activated ester of Cy5 (Lumiprobe, Hunt Valley, MD, USA). Covalent attachment was achieved by reacting 25 μL of 50 mg mL^{-1} NHS-Cy5 (5 equiv per CP) with 10 mg of CPMV in 0.01 M KP buffer on an orbital shaker for 2 h at room temperature. The Cy5-CPMV conjugate was continuously purified using a 100 kDa molecular weight cutoff (MWCO) centrifugal filter (500*g*, 5 min, room temperature) until a clear filtrate was obtained. The concentration of Cy5-CPMV particles was determined by UV−vis spectrophotometry as described above, and the Cy5 absorption at 647 nm ($\varepsilon_{647\ nm}$ = 271 000 L mol^{-1} cm^{-1}) was used to estimate the dye loading per particle.

Conjugation of CPMV to Epitope 826. CPMV particles were labeled with the bifunctional PEGylated cross-linker SM(PEG)$_4$ (Thermo Fisher Scientific) using a reactive NHS-activated ester that targets lysine residues. The reaction was performed by mixing 2000-fold molar excess of SM(PEG)$_4$ with 2 mg of CPMV particles in 0.01 M KP buffer for 2.5 h at room temperature. The PEGylated intermediate was purified using a 100 kDa MWCO centrifugal filter (16 000*g*, 5 min, 4 °C). The maleimide handles of the PEGylated intermediate were then reacted with the cysteine residue of epitope 826 (GenScript Biotech, Piscataway, NJ, USA) by mixing 2 mg of PEGylated CPMV with 0.2 mL of 20% Pluronic F-127 (MilliporeSigma, Burlington, MA, USA) in DMSO[69] and then adding 0.12 mL of 20 mg mL^{-1} epitope 826 in DMSO and stirring overnight. The 826-CPMV conjugate was purified by centrifugation on a 0.1 mL 40% sucrose cushion (50 000 rpm, 1 h, 4 °C) and dialysis against 0.01 M KP buffer for 24 h at room temperature. The 826-CPMV particles were concentrated using a 100 kDa MWCO centrifugal filter (8000*g*, 5 min, 4 °C) and quantified by UV−vis spectrophotometry as described above. They were also visualized by transmission electron microscopy (TEM) on a Tecnai F30 instrument (FEI Company, Hillsboro, OR, USA) after staining with 2% uranyl acetate.

Characterization of CPMV Nanoparticles. *Size Exclusion Chromatography.* We loaded 200 μg of CPMV particles onto a Superose6 column in the ÄKTA Explorer chromatography system (GE Healthcare, Chicago, IL, USA) and eluted them with 0.1 M KP buffer (pH 7.0) at a flow rate of 0.5 mL min^{-1}. The capsid protein, viral RNA, and conjugated Cy5 dye were detected at 260, 280, and 647 nm, respectively.

Dynamic Light Scattering. We determined the hydrodynamic diameter, polydispersity index (PDI), and zeta potential of the particles using a Zetasizer Nano ZSP Zen5600 instrument (Malvern Panalytical, Malvern, UK). Triplicate measurements were acquired over 3−5 min at room temperature with a scattering angle of 90°.

Native Gel Electrophoresis. Particles (10−20 μg) suspended in Tris/Borate/ethylenediaminetetraacetic acid (EDTA) (TBE) buffer (45 mM Tris, 45 mM boric acid, 1.25 mM EDTA in Milli-Q water) were loaded onto 1.2% agarose gels and fractionated for 30 min at 120 V and 400 mA. The gels were documented on an AlphaImager (Protein Simple, San Jose, CA, USA) under UV, red, and white light before and after staining with Coomassie brilliant blue (CBB).

Sodium Dodecylsulfate Polyacrylamide Gel Electrophoresis. Protein samples (10 μg) were analyzed side by side with SeeBlue Plus2 prestained protein standards (Thermo Fisher Scientific) on 4−12 or 12% NuPAGE polyacrylamide gels using 1× MOPS elution buffer (Invitrogen, Thermo Fisher Scientific) at 200 V and 120 mA for 40 min. Gel images were documented on the AlphaImager system under red and white light before and after CBB staining.

Hydrogel Formulation and Characterization. *Preparation of Chitosan/GP Formulations.* Liquid formulations were prepared by mixing the chitosan and GP solutions and vortexing the mixture with the CPMV, Cy5-CPMV, or 826-CPMV particles. The chitosan solution was prepared by dispersing 4 g of chitosan powder (Chem-Impex International, Wood Dale, IL, USA) in 180 mL of 0.1 M HCl for 2 h, followed by autoclaving for 20 min at 121 °C and homogenization by stirring overnight at room temperature.[70] We prepared chitosan solutions of low molecular weight (LMW, 250 kDa), medium molecular weight (MMW, 1250 kDa), and high molecular weight (HMW, 1500 kDa). The GP solution was prepared by dissolving 5.60 g of β-glycerophosphoric acid disodium salt (MilliporeSigma) in 10 mL of deionized water and passing the solution through a 0.22 μm filter. The chitosan and GP solutions were mixed at a 5:1 (v/v) ratio,[63] and different amounts of CPMV in phosphate-buffered saline (PBS) were dispersed by vortexing to yield 0 (blank), 2.25 (0.225%), and 4.5 mg mL^{-1} (0.450%) CPMV nanoparticles in the final formulations (Table 1). Minitab v13

Table 1. Formulation Parameters for the Design of CPMV/Chitosan/GP Hydrogels

level	chitosan molecular weight (MW)	final CPMV concentration, mg mL^{-1} (%)
1	low MW (250 kDa)	0 (0%)
2	medium MW (1250 kDa)	2.25 (0.225%)
3	high MW (1500 kDa)	4.5 (0.45%)

(Minitab, Coventry, UK) was used for the factorial design of nine different formulations for evaluation against gelation time. CPMV 0.45% was duly selected, and the Cy5-CPMV formulations were prepared as follows: chitosan/GP solutions were vortexed with 15 mg mL^{-1} Cy5-CPMV at a 7:3 (v/v) ratio yielding 0.45% formulations denoted F1, F2, and F3 representing the LMW, MMW, and HMW chitosan, respectively. Formulation F3 based on HMW chitosan achieved the shortest gelation time and prolonged release profiles and was therefore used to encapsulate 826-CPMV as described for Cy5-CPMV. Blank hydrogels were prepared under the same conditions using PBS-lacking CPMV particles.

Viscosity Measurements. Viscosity was measured using a parallel plate ARG2 rheometer (TA Instruments, New Castle, DE, USA). We pipetted 200 μL of each sample into the center of the parallel plate geometry, which was set at 25 °C with a gap height of 500 μm (ensuring the liquid covered the entire gap between the plates).

Determination of the Gelation Time Using the Tube Inversion Method. We incubated 1 mL of each sample (in a 1.5 mL Eppendorf tube) at 37 °C and inverted the tube every 60 s. The gelation time point was recorded when the formulation no longer flowed in the inverted tube after 30 s[65]

Hydrogel Swelling and Degradation In Vitro. We incubated 0.5 mL of each hydrogel sample containing Cy5-CPMV (in a 1.5 mL Eppendorf tube) at 37 °C for 45 min to ensure complete gelation. The initial height of the gel was measured before carefully adding 1 mL of PBS and agitating the tubes at 200 rpm. At predefined time intervals, the liquid phase was removed and set aside for Cy5-CPMV characterization. We added the same amount of fresh PBS and recorded the height of gel to calculate the swelling ratio (the height at any time divided by the initial height × 100).[65] Following this longitudinal incubation in PBS, exhausted gels (and fresh gels) were freeze-dried and imaged by scanning electron microscopy (SEM) using a Quanta 600 ESEM (FEI Company) operating at 10 kV.

Characterization of Cy5-CPMV Released from Hydrogels In Vitro. The liquid phase set aside from the previous step was compared to a defined amount of Cy5-CPMV in PBS as a control. Fluorescence measurements were recorded on a microplate reader (Tecan, Männedorf, Switzerland) to quantify Cy5 (λ_{Ex} = 600 nm, λ_{Em} = 665 nm) and estimate Cy5-CPMV release profiles.[66] The particles were separated by sodium dodecylsulfate polyacrylamide gel electrophoresis (SDS-PAGE) to confirm the molecular stability of the Cy5-CPMV CP conjugates. The intactness of the particles was confirmed by native gel electrophoresis and TEM as described above.

Animal Experiments. *Ethical Statements.* Animal procedures were carried out according to the guidelines of the Institutional Animal Care and Use Committee of the University of California San Diego (UCSD) following the protocols approved by the Animal Ethics committee of UCSD. For all animal experiments, we used healthy BALB/c female mice (7−8 weeks old) purchased from the Jackson Laboratory (Bar Harbor, ME, USA) and hosted at the UCSD Moores Cancer Center with unlimited food and water.

Characterization of Cy5-CPMV Released from Hydrogels In Vivo. Hydrogel formulations F1−F3 (100 μL, containing 450 μg of Cy5-

https://doi.org/10.1021/acs.biomac.2c00112
Biomacromolecules 2022, 23, 1812−1825

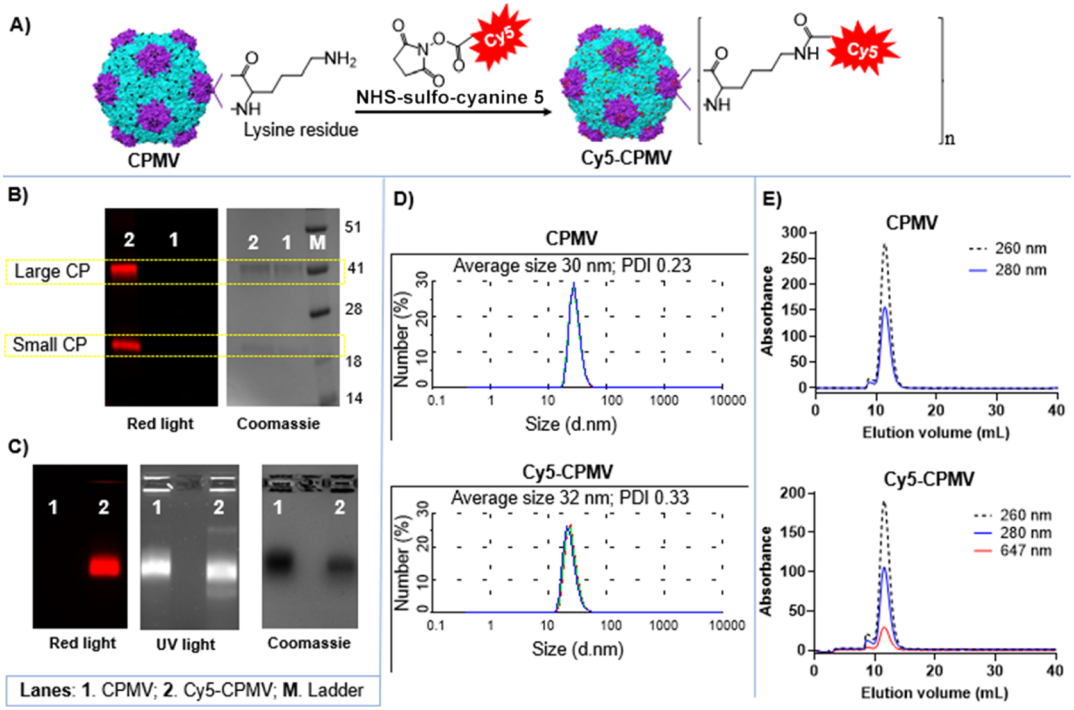

Figure 1. Characterization of CPMV and Cy5-CPMV. (A) Bioconjugation reaction, labeling of CPMV with sulfo-Cy5 using NHS chemistry. Black dots on the CPMV surface represent lysine residues. (B) SDS-PAGE comparing CPMV wild-type and Cy5-conjugated CPs, demonstrating similar electrophoretic profiles and thus successful covalent attachment. (C) Native agarose gel electrophoresis demonstrating the similar electrophoretic mobility of CPMV/Cy5-CPMV (viral proteins, RNA, and Cy5 fluorophore), suggesting that the particles are intact. (D) DLS measurements indicating the nanoparticulate nature of CPMV/Cy5-CPMV samples. (E) Size-exclusion chromatography confirming the CPMV/Cy5-CPMV particle integrity by the coelution of all viral components in the same peak. The black dashed curve represents viral CP absorbance at λ = 260 nm, the blue solid curve is the RNA signal at λ = 280 nm, and the red solid line is Cy5 detected at λ = 647 nm.

CPMV) or soluble Cy5-CPMV (450 μg in 100 μL of PBS) were administered as single subcutaneous injections behind the neck of shaved mice on day 0 (five mice per group). Animals were maintained on an alfalfa-free diet 1 week before the experiment and throughout the study to prevent tissue autofluorescence. The injection site was imaged at different time points under a Xenogen IVIS 200 Optical Imaging System (Caliper Life Sciences, Hopkinton, MA, USA). IVIS software was used to determine the fluorescence intensity within a region of interest (ROI) and thus evaluate the persistence of fluorescence as a marker of slow release. The F3 formulation (200 μg single subcutaneous injection) was then selected for comparison to 2 × 100 μg doses of soluble Cy5-CPMV.

Immunization Procedure. BALB/c female mice (four mice per group) were assigned to one of the following treatment groups, with all treatments involving subcutaneous injections behind the neck: (i) group 100 = prime-boost (week 0 and week 2) injections of 100 μg of soluble 826-CPMV in 150 μL of PBS; (ii) group 200 = single injection of 200 μg of soluble 826-CPMV in 150 μL of PBS; (iii) group F3 = single injection of the F3 formulation containing 200 μg of 826-CPMV; and (iv) group blank F3 = single injection of the F3 formulation without 826-CPMV. Blood samples were collected by retro-orbital bleeding before injection (week 0) and on weeks 2, 4, 8, 12, 16, and 20. Blood samples were centrifuged (2000*g*, 10 min, 4 °C), and the plasma was kept at −80 °C for antibody screening.

Enzyme-Linked Immunosorbent Assay. Anti-826 antibodies were detected by enzyme-linked immunosorbent assay (ELISA) as previously reported.[39] Pierce maleimide-activated 96-well plates (Thermo Fisher Scientific) were rinsed three times with 200 μL per well of PBS containing 0.05% (v/v) Tween-20 (PBST), and the same washing procedure was used between all subsequent steps. The washed plates were coated with peptide epitope 826 (20 μg mL^{-1}, 100 μL per well) in binding buffer (0.1 M sodium phosphate, 0.15 M sodium chloride, 0.01 M EDTA, pH 7.2) overnight at 4 °C. After discarding the coating solution and washing the plates, each well was blocked with 100 μL of 10 μg mL^{-1} cysteine in binding buffer, and the plates were incubated at room temperature for 1 h. Following the blocking step, the plasma from immunized animals was added in PBS (100 μL per well) using dilution factors of 200, 400, 800, 1600, 3200, 6400, 12,800, 25,600, 51,200, 102,400, and 204,800. After incubating for 1 h at room temperature and washing, we added the horseradish peroxidase (HRP)-conjugated goat antimouse IgG Fc-specific secondary antibody (Invitrogen, diluted 1:5000) in PBST and incubated the plates again for 1 h at room temperature. Following another wash, we added 100 μL per well of the 1-Step Ultra TMB-ELISA substrate (Thermo Fisher Scientific) and allowed the plates to develop for 5 min at room temperature before stopping the reaction with 100 μL per well of 2 N H_2SO_4 and reading the optical density at 450 nm on a Tecan microplate reader.

Antibody Isotyping. The ELISA protocol for anti-826 antibody screening was slightly modified for the isotyping experiment. Instead of serial dilutions, samples from weeks 4 and 12 were diluted 1:1000 in binding buffer. As secondary antibodies, we used HRP-conjugated goat anti-mouse IgG1 (Invitrogen PA174421, 1:5000), IgG2a (Invitrogen A-10685, 1:1000), IgG2b (Abcam, Cambridge, UK, ab97250, 1:5000), IgG2c (Abcam ab9168, 1:5000), IgG3 (Abcam ab98708, 1:5000), IgE (Invitrogen PA184764, 1:1000), and IgM (Abcam ab97230, 1:5000). The IgG1/IgG2a ratio was calculated, with values < 1 considered indicative of a Th1 response and values > 1 considered indicative of a Th2 response.

Statistical Analysis. Graphical data were processed and analyzed using GraphPad Prism v9.0.2 (GraphPad Software, San Diego, CA, USA), unless otherwise indicated. Depending on the datasets, data were statistically compared by one-way analysis of variance (ANOVA) followed by Tukey's multiple comparison test or two-way ANOVA using pairwise multiple comparison followed by a posttest Holm−Šidák correction. Asterisks in figures indicate significant differences between groups (*p < 0.05; **p < 0.01; ***p < 0.001; ****p < 0.0001).

https://doi.org/10.1021/acs.biomac.2c00112
Biomacromolecules 2022, 23, 1812−1825

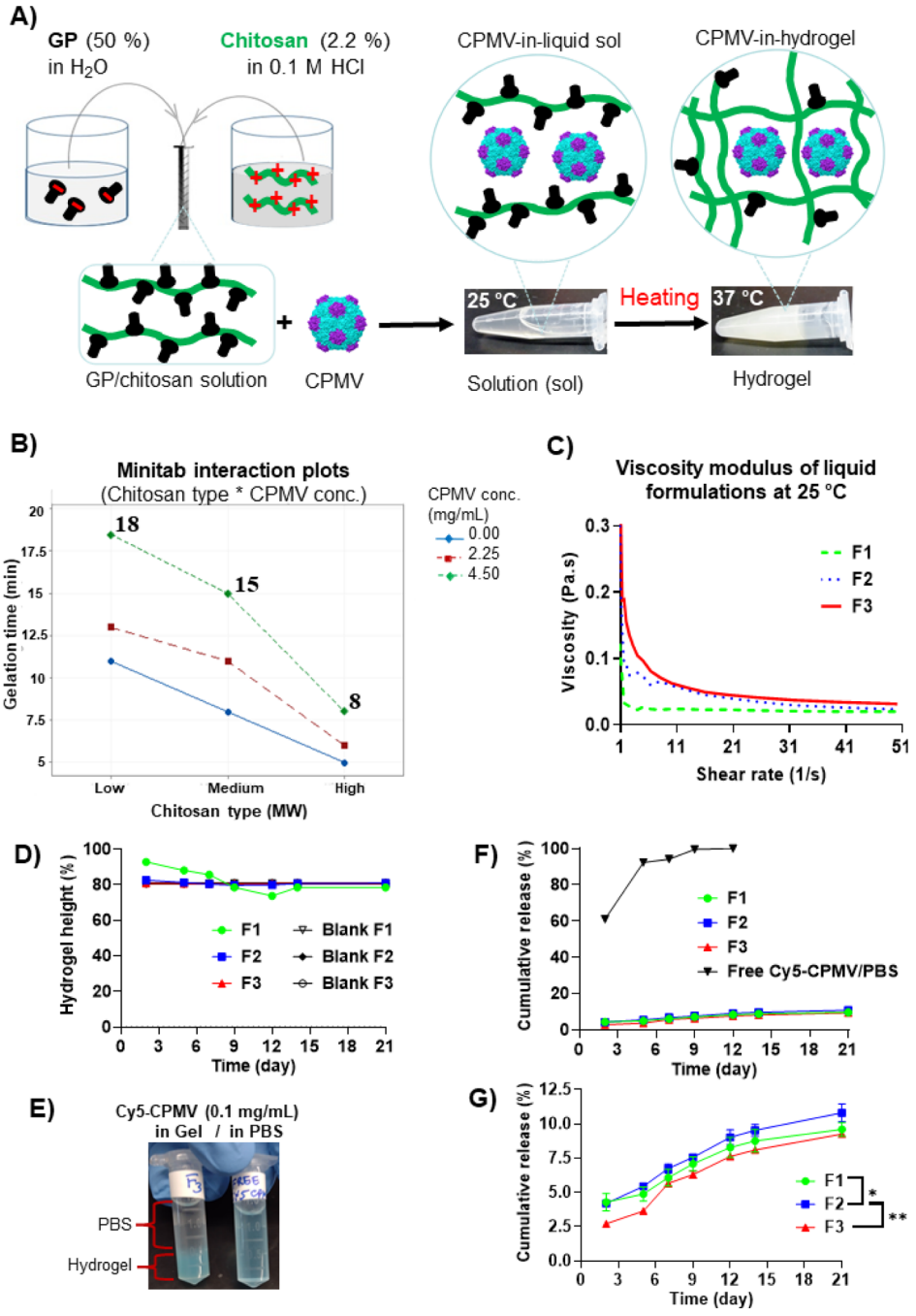

Figure 2. Preparation and characterization of hydrogels. (A) CPMV particles were dispersed in chitosan/GP hydrogels. (B) Design-of-experiment plots (from Minitab software) showing the impact of two formulation variables (chitosan molecular weight and CPMV concentration) on gelation time. (C) Rheological properties of liquid formulations, showing variations in relative viscosity at 25 °C. (D) Gel height variations measured at different time points following hydrogel incubation in PBS at 37 °C ($n = 3$). (E) Experimental setting used for in vitro gel swelling/degradation and release analysis, showing the homogeneous dispersion of Cy5-CPMV in hydrogel F3 vs PBS. (F) Full data set showing in vitro Cy5-CPMV release from hydrogels vs soluble Cy5-CPMV/PBS at 37 °C ($n = 3$). (G) Release data excerpt showing the difference between the three hydrogel formulations. Asterisks indicate significant differences between groups (*$p < 0.05$; **$p < 0.01$).

RESULTS AND DISCUSSION

Preparation and Labeling of CPMV Particles. CPMV was purified from infected black-eyed pea plants yielding 0.55 mg per gram of leaf tissue. The 260/280 nm absorbance ratio was 1.75, well within the 1.7−1.8 range anticipated for pure particles.[68] Surface-exposed lysine side chains were conjugated to Cy5 using NHS chemistry (Figure 1A). Five equivalents of NHS-sulfo-Cy5 per CP achieved a loading efficiency of 19 Cy5 molecules per particle, which is acceptable for fluorescence imaging.[71] SDS-PAGE and native agarose gel electrophoresis confirmed the attachment of Cy5 (Figure 1B,C). Illumination of the polyacrylamide gels with red light revealed fluorescent bands matching the small and large CP bands on gels stained with CBB, indicating that Cy5 was covalently linked to both polypeptides. Illumination of the native agarose gels under red light showed a fluorescent band matching the UV band (RNA signal) and the protein band on gels stained with CBB (intact

https://doi.org/10.1021/acs.biomac.2c00112
Biomacromolecules 2022, 23, 1812−1825

particles), thus confirming that the particles were intact following bioconjugation. This was consistent with size analysis by dynamic light scattering (DLS), which showed the presence of nanometer-scale particles in the CPMV and Cy5-CPMV samples (Figure 1D). Particle integrity was verified by the single elution peak during size-exclusion chromatography: proteins were detected at 260 nm, RNA at 280 nm, and Cy5-CPMV at 647 nm (Figure 1E). The latter also confirmed the absence of aggregates, broken particles, free proteins, or free dye molecules.

Preparation and Characterization of Hydrogels Loaded with CPMV/Cy5-CPMV. *Gel Formation.* Chitosan is soluble in acids due to the electrostatic repulsion between its positively charged amine-protonated chains. The addition of GP neutralizes the solution (pH = 6.5−7.3) without inducing immediate precipitation or aggregation because GP deprotonates some of chitosan's positively charged amine groups ($-NH_3^+$), allowing electrostatic attraction between the GP backbone and chitosan's remaining $-NH_3^+$ groups, in turn exposing the glycerol moiety of GP to neighboring chitosan chains and enhancing their solubility when the temperature is below ∼23 °C.[56,72] Higher temperatures trigger the transfer of protons from chitosan's $-NH_3^+$ groups to the GP backbone, reducing the charge density of chitosan and favoring hydrophobic interchain interactions and hydrogen bonding between chitosan chains, resulting in the formation of a gel.[57,58,72,73]

We investigated the gelling behavior of chitosan/GP mixtures featuring three different molecular weights of chitosan (LMW = 250 kDa, MMW = 1250 kDa, and HMW = 1500 kDa) and various concentrations of CPMV (0−4.5 mg mL^{-1}) at 37 °C. The gelation time was assessed by the flow and turbidity of each mixture following tube inversion (Figure 2A). The gelation time decreased with increasing chitosan molecular weight, but the concentration of CPMV was also relevant (Figure 2B and Table S2). This is consistent with previous studies demonstrating that solution-to-gel transition is influenced by many formulation parameters, including chitosan molecular weight and cargo loading.[74] Blank formulations gelled much faster than those containing CPMV, supporting previous observations that nanoparticles occupy the space between chitosan chains and slow gelation.[66] The shortest gelling time was observed for the formulations containing HMW chitosan (5−8 min). We selected the formulations with the highest load of CPMV (4.5 mg mL^{-1}) for further characterization because this allows the maximum dosage with the smallest volume of the excipient. The formulations containing 4.5 mg mL^{-1} CPMV dispersed in LMW, MMW, and HMW chitosans were named F1, F2, and F3, respectively. The liquid formulation F3 was the most viscous (0.482 Pa·s), 2.4-fold more viscous than F2 (0.202 Pa·s) and 4.8-fold more than F1 (0.099 Pa·s). The viscosity modulus of F1 (and to some degree F2) decreased abruptly as the shear rate increased, whereas the viscosity modulus of F3 declined gradually (Figure 2C). This indicates much better shear-thinning and self-healing behavior,[62] reflecting the presence of stronger interchain interactions as would be anticipated from the short gelation time.

Gel Swelling, Degradation, and In Vitro Release Profiles. Next, we assessed gel swelling and degradation, as well as the Cy5-CPMV release profile over 21 days in PBS at 37 °C. Although hydrogel F1 initially showed some fluctuations (Figure 2D), all formulations ultimately showed no significant change in the gel height (Figure 2E). The apparent volume of the gel therefore remained constant regardless of the composition (loaded with Cy5-CPMV particles or blank). This agrees with one earlier report,[65] but in another case, the authors observed significant height fluctuations.[75] The constant apparent volume of our gel suggests that the rates of gel swelling and degradation are comparable, which implies a robustness that may interfere with cargo release. However, SEM revealed that the microstructure of fresh (nonincubated) hydrogels comprised a bulky but porous matrix, which would encourage cargo release even without degradation (Figure S1). SEM images of the exhausted gels (after incubation in PBS) included abundant salt crystals, which made it difficult to determine the matrix structure (data not shown). Despite these results, the slow-release capability of the hydrogels was confirmed directly by measuring the quantity of Cy5-CPMV particles in the liquid phase (Figure 2E). The gels remained stable throughout the 21 days of testing, but we observed the gradual release of Cy5-CPMV nanoparticles from all formulations, suggesting that the particles can diffuse through the pores identified above (Figure 2F,G). The slowest release profile was observed for F3, consistent with its rapid gelation and high viscosity, followed by F1 and then F2. This suggests that the release profile is not directly related to the molecular weight of the chitosan. We found that a free suspension of Cy5-CPMV released 100% of the particles after incubation in PBS for 10 days, which was anticipated because the particles can move freely due to Brownian motion. In contrast, only 10−12% of the particles were released from the hydrogels after 21 days, reflecting a combination of physical obstruction and chemical interactions within the gel matrix.[76,77]

Characterization of Cy5-CPMV Released from the Hydrogels In Vitro. Having established the potential for intermolecular interactions within the hydrogel, we investigated whether the chemical reactivity of the matrix had a negative impact on nanoparticle stability. Cy5-CPMV particles released from the hydrogels on days 7 and 14 were characterized by native agarose gel electrophoresis, SDS-PAGE, and TEM. The illumination of agarose gels with red light revealed Cy5 bands that matched the RNA signal under UV light and the protein bands under white light following staining with CBB (Figure S2A). This confirmed the presence of intact particles containing all three components. Some particles remained in the loading wells, which may reflect particle aggregation or interactions with positively charged chitosan molecules affecting electrophoretic migration toward the anode. The chemical stability of the Cy5-CP conjugates was confirmed by SDS-PAGE, which showed that the protein bands corresponding to the small and large CPs after staining with CBB appeared at the same positions as the fluorescent bands representing Cy5 (Figure S2B). This confirmed that the covalent linkage between Cy5 and the particles remained stable after 14 days in the hydrogel matrix. Finally, the structural integrity of the Cy5-CPMV particles eluted from hydrogels was confirmed by TEM (Figure 3). Taken together, these observations suggest that chemically modified CPMV nanoparticles are likely to maintain their particulate and molecular integrity following encapsulation within and release from the chitosan/GP hydrogels.

In Vivo Retention and Release Profiles. Cy5-CPMV-loaded formulations F1, F2, and F3 were injected subcutaneously behind the neck of shaved BALB/c mice to determine the retention and release profiles in vivo. Cy5-CPMV in PBS was

https://doi.org/10.1021/acs.biomac.2c00112
Biomacromolecules 2022, 23, 1812−1825

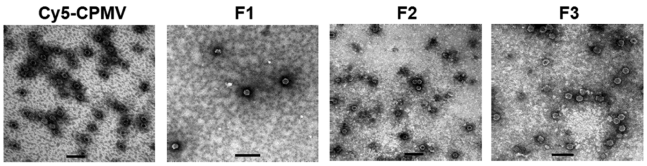

Figure 3. TEM images of Cy5-CPMV released in vitro from hydrogels following incubation in PBS for 14 days, confirming the integrity and stability of Cy5-CPMV particles within the hydrogel matrix.

injected as a control. The local retention of Cy5-CPMV was assessed over 21 days by fluorescence imaging of the injection site and ROI analysis. The signals from the single dose of soluble Cy5-CPMV decayed rapidly compared to those from the hydrogel formulations, disappearing almost completely by day 12 postinjection due to fast diffusion and clearance[62] (Figure 4A). The signals from F1 and F2 lasted until day 18, and the signal from F3 was still present at the end of the experiment, indicating depot formation in situ followed by the slower diffusion of Cy5-CPMV from the injection site. Although the hydrogel significantly increased the residence time of CPMV, the excellent tissue residence time of the soluble formulation is also notable, probably reflecting the high stability of the CPMV nanoparticles. Quantitative fluorescence intensity analysis revealed that F3 was the only formulation that differed significantly from free Cy5-CPMV in terms of fluorescence decay (Figure 4B). This agrees with the observed ability of F3 to outperform the other formulations in vitro (e.g., the shortest gelation time and slower release). We also compared Cy5-CPMV local retention following subcutaneous injections of F3 (200 μg single dose) versus soluble Cy5-CPMV (100 μg every 14 days), and the outcome was intriguing. Bright fluorescence at the injection site was observed in both groups on day 15 but only in the F3 group on day 28, confirming the prolonged tissue residence due to depot formation (Figure 4C). Although the reliability of fluorescence signals is limited by the potential for quenching or particle aggregation (especially in the confined subcutaneous injection site), the results nevertheless allowed us to compare

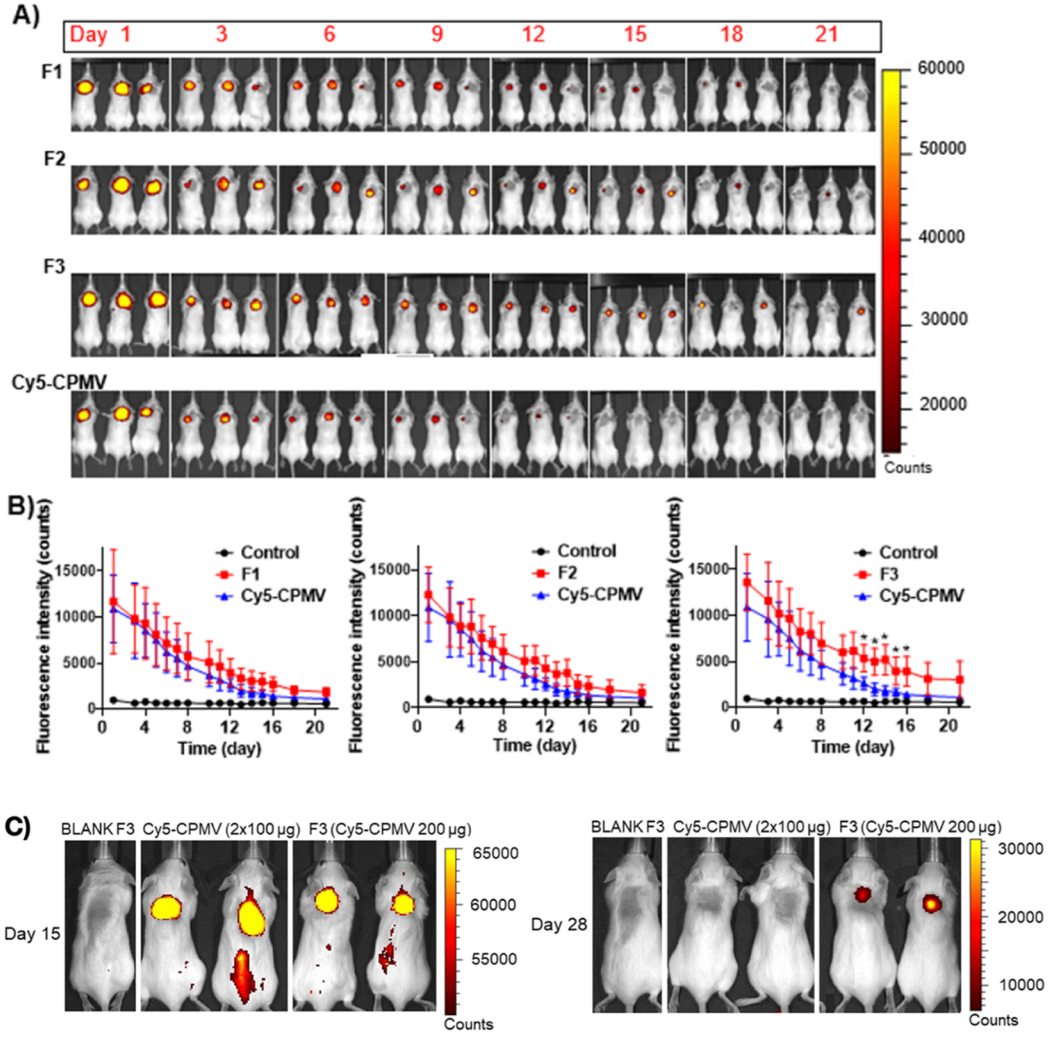

Figure 4. In vivo retention/release of Cy5-CPMV from hydrogels (F1, F2, and F3) vs soluble Cy5-CPMV. (A) Fluorescence images and (B) fluorescence intensity at the injection site in female BALB/c mice (n = 5 per group) following a single subcutaneous injection of F1, F2, or F3 (450 μg of Cy5-CPMV) or soluble Cy5-CPMV (450 μg) on day 0. Asterisks indicate significant differences between F3 and Cy5-CPMV (*p < 0.05). (C) Comparing local retention of a single subcutaneous dose of hydrogel F3 (containing 200 μg of Cy5-CPMV) vs two doses of soluble Cy5-CPMV (100 μg injected at days 0 and 14) in female BALB/c mice. Fluorescence images demonstrating the extended tissue residence of the F3 hydrogel compared to that of the soluble Cy5-CPMV.

https://doi.org/10.1021/acs.biomac.2c00112
Biomacromolecules 2022, 23, 1812−1825

the rate of Cy5-CPMV particle clearance when using soluble and slow-release formulations, supporting the enhanced local retention achieved by the administration of Cy5-CPMV in chitosan/GP hydrogels.[78]

Efficacy of 826-CPMV-Loaded Hydrogel as a Single-Dose Vaccine. *Bioconjugation of Peptide Epitope 826 to CPMV.* We conjugated the B-cell epitope 826 (peptide sequence 809−826 of the SARS-CoV-2 S protein) to CPMV using our two-step protocol as previously described.[39] This peptide is highly conserved and is not affected by the mutations that generated the Delta and Omicron variants of SARS-CoV-2 (Figure S3). We used NHS chemistry to attach the cross-linker $SM(PEG)_4$ to lysine side chains on CPMV (Figure 5A). The resulting maleimide handles were quickly

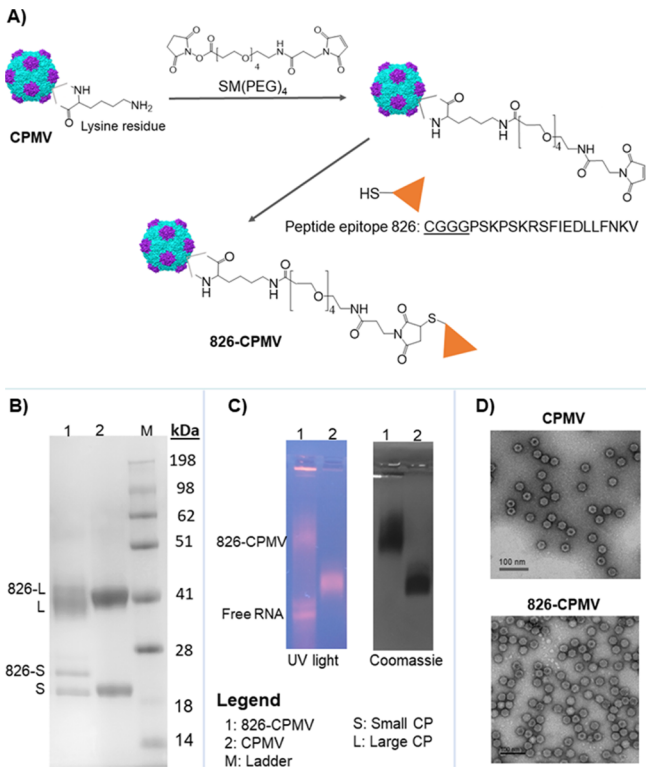

Figure 5. Conjugation of the B-cell peptide epitope 826 to CPMV. (A) Two-step synthesis of 826-CPMV conjugates. (B) SDS-PAGE analysis comparing the CPs from wild-type and modified CPMV particles. (C) Agarose gel showing the colocalization of viral RNA (under UV light) with CP (revealed by staining with CBB). (D) TEM images confirming particle integrity following the bioconjugation reaction. Scale bar = 100 nm.

conjugated to the cysteine residues of peptide 826 in the presence of the polymer Pluronic F127, a surfactant used for peptide solubilization.[69] The 826-CPMV particles were purified by ultracentrifugation and characterized by SDS-PAGE, native agarose gel electrophoresis, and TEM. SDS-PAGE revealed the presence of new CP bands with higher molecular weights than those of the native small and large CPs, reflecting the conjugation of the additional peptide (Figure 5B). Quantitative analysis by densitometry indicated that each nanoparticle displayed ∼60 peptide epitopes, which is in agreement with our previous study.[39] Native agarose gel electrophoresis indicated that the 826-CPMV particles had a lower electrophoretic mobility than native CPMV, which can be attributed to the higher molecular weight and increase in hydrodynamic diameter (Figure 5C). The presence of a higher-mobility band that appeared to be free RNA (stained with GelRed but not with CBB) may indicate the release of RNA under the reaction conditions, in agreement with our previous work on the 826-CPMV formulation.[69] While some RNA is lost during the conjugation procedure, a significant amount of the RNA is retained within the formulation. Importantly, RNA is not lost during hydrogel formulation (see Figure S2). The structural integrity of the 826-CPMV nanoparticles was confirmed by TEM, which revealed homogeneous icosahedral particles of ∼30 nm (Figure 5D). Collectively, these data confirmed the synthesis of stable 826-CPMV nanoparticles for immunization studies.

Immunogenicity of Hydrogel F3 Containing 826-CPMV Particles. The immunogenicity of 826-CPMV formulated in chitosan/GP hydrogel F3 was evaluated in female BALB/c mice. Based on the previously reported dosing schedule for 826-CPMV,[39] a single dose of liquid formulation F3 containing 200 μg of 826-CPMV particles was compared with the soluble particles in PBS administered as a single subcutaneous dose of 200 μg or prime-boost doses of 100 μg at the beginning of weeks 0 and 2 (Figure 6A). Blood samples were collected by retro-orbital bleeding over 20 weeks and sera were screened for antibodies against epitope 826 by ELISA (Figure 6B). The control group (F3 hydrogel without 826-CPMV particles) did not elicit antibodies, whereas all study groups produced anti-826 IgG (Figure 6C). The injectable hydrogel formulation of 826-CPMV improved the antibody titers at later time points (between weeks 12 and 20) compared to the soluble formulation (Figure 6D). Significantly high antibody concentrations were still apparent at week 20 following the administration of 826-CPMV particles in hydrogel F3. Differences in antibody titers were apparent at later time points with higher titers observed in animals immunized with the 826-CPMV particles released from the F3 hydrogel versus single administration of 200 μg of 826-CPMV particles or prime-boost with 100 μg of 826-CPMV particles (Figure 6C,D). This is consistent with the prolonged tissue residence time and slow release of CPMV from the injectable hydrogel compared to the faster clearance of the soluble CPMV formulation (Figure 4). The data provide further evidence that intact and biologically active CPMV nanoparticles released from the hydrogel retained their biological properties, supporting the in vitro stability data (Figures 3 and S2). The chitosan/GP slow-release technology is therefore highly compatible with plant virus nanotechnology. Our results are important because many nations have now initiated repeat vaccinations with shorter intervals in an attempt to control COVID-19, whereas a slow-release formulation could provide long-lasting immunity by creating a depot that releases vaccine antigens over a period of several months. The use of such formulations would therefore alleviate some of the burden on global health systems by reducing the number of vaccination appointments needed to achieve population-wide protection.

Antibody Isotyping. Finally, we analyzed the Ig isotypes and IgG subclasses in plasma from weeks 4 and 12 and thus reveal whether hydrogel vaccine F3 induced a Th1-biased response (IgG1/IgG2a ratio < 1) or a Th2-biased response (IgG1/IgG2a ratio > 1). Th1 cells produce cytokines such as interferon γ that instruct B cells to produce opsonizing antibodies (IgG2a/b) and stimulate macrophages for phagocytic activity against intracellular pathogens (e.g., viruses). In contrast, Th2 cells produce interleukin 4 (IL-4) that instructs

https://doi.org/10.1021/acs.biomac.2c00112
Biomacromolecules 2022, 23, 1812−1825

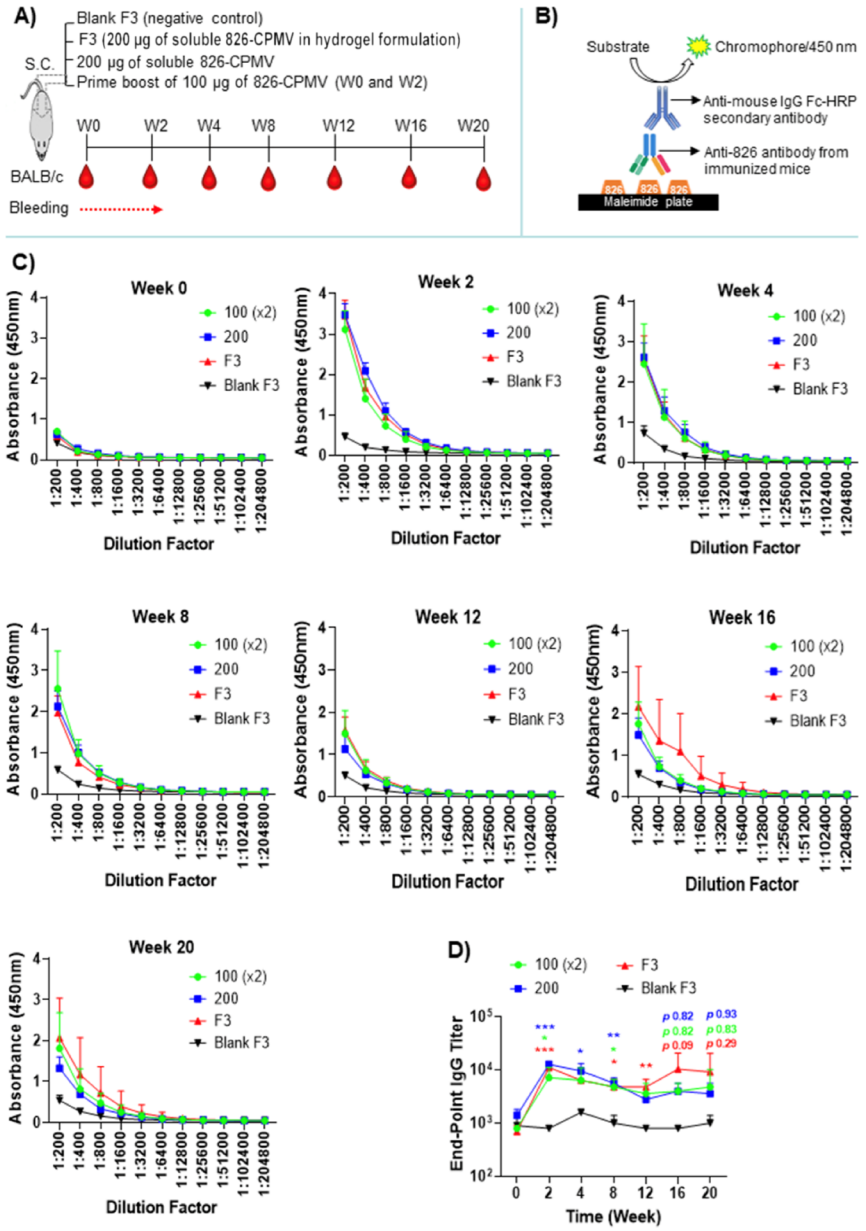

Figure 6. Antibody response following the immunization of BALB/c mice (n = 4 per group). (A) Mice were subcutaneously injected once with hydrogel F3 (containing 200 μg of 826-CPMV) or 200 μg of soluble 826-CPMV in PBS or with 2 × 100 μg of soluble 826-CPMV in PBS as a prime-boost regimen. Blood samples were withdrawn by retro-orbital bleeding according to the schedule as shown. (B) ELISA detecting IgG (from immunized mouse serum) binding to epitope 826. (C) ELISA data curves showing IgG titers of immunized mice against epitope 826 from weeks 2 to 20. (D) Longitudinal IgG titers over 20 weeks indicating that the F3 group continuously differed from the control blank group to a much greater extent than the soluble particle (with p values included for weeks 16 and 20 to show the differences). Asterisks indicate significant differences between the study group and control blank group (*p < 0.05; **p < 0.01; ***p < 0.001; ****p < 0.0001), with green color referring to the soluble 826 CPMV 100 (x2) group, blue to the 826 CPMV 200 group, and red to the F3 group.

B cells to secrete neutralizing antibodies (IgG1) for humoral protection against pathogens or toxins in the extracellular environment.[40] We observed comparable Ig isotype profiles in all groups at week 4 but evident differences at week 12 due to IgG1 becoming exclusively prominent in the F3 group (red arrows in Figure 7A). Based on the IgG1/IgG2a ratio, we found that F3 induced a Th1-biased response at week 4 but shifted to a Th2-biased response at week 12, while the immune response for the soluble 826-CPMV groups remained Th1-biased throughout the experiment (Figure 7B). CPMV-based vaccines were previously shown to induce Th1-biased responses against cancers,[41,79,80] but Th2-biased responses at later time points have been reported for other shared epitopes from SARS-CoV and the SARS-CoV-2 S protein, reflecting a shift from Th1 typically after the second boost injection.[43] The Th1/2 response was deemed to be dependent on the SARS-CoV2 S protein epitope.[39,43] With regard to epitope 826, we and others[39] observed only Th1-biased responses for soluble 826-CPMV administered using the prime-boost schedule, which implies that the observed shifting bias in the F3 group from Th1 to Th2 is possibly due to the immune-enhancing adjuvant capability of chitosan[53−55,81] and/or the slow-release characteristics of the hydrogel F3. The first CPMV nanoparticles released from the gel can diffuse through lymph vessel

https://doi.org/10.1021/acs.biomac.2c00112
Biomacromolecules 2022, 23, 1812−1825

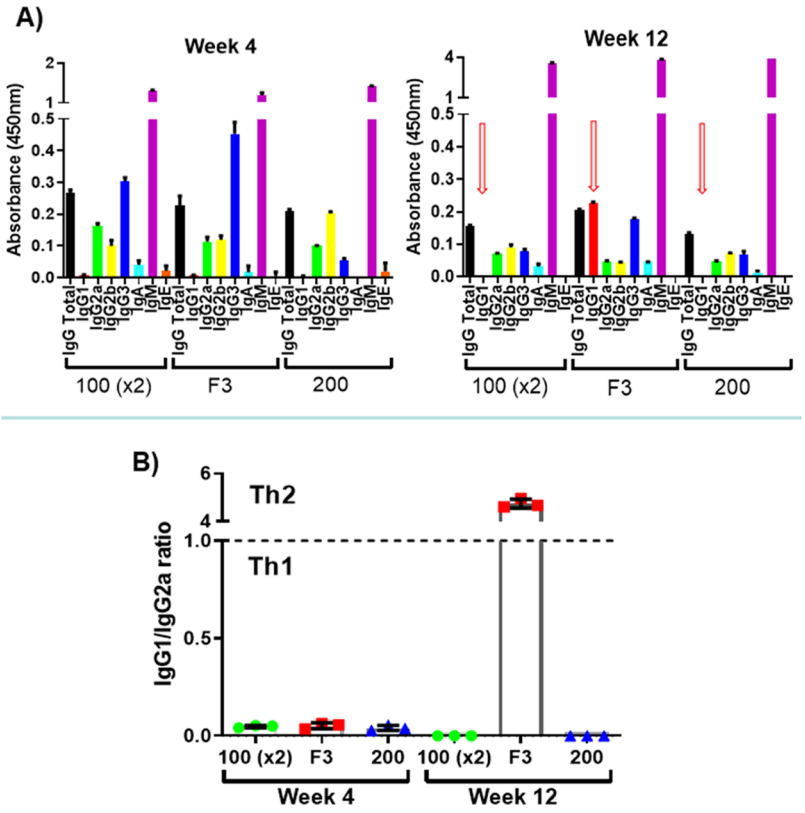

Figure 7. Antibody isotyping using mouse sera from weeks 4 and 12 (n = 4 per group). (A) Immunoglobulin isotypes and IgG subclasses, showing comparable antibody profiles at week 4 but enhanced IgG1 production by the F3 group at week 12 (three red arrows). (B) IgG profiling expressed as the IgG1/IgG2a ratio, demonstrating a Th1-biased response (IgG1/IgG2a ratio < 1) for all groups at week 4 but a remarkable shift to a Th2-biased response (IgG1/IgG2a ratio > 1) exclusively in the F3 group.

pores and find their way to the lymph node, where they interact directly with B cells to induce immediate IgG2a production (Th1 bias) without prior interactions with T cells.[40,82] However, longitudinal and delayed release may induce more Th2 bias because the particles are likely to interact with antigen-presenting cells due to their prominent recognition by pre-existing opsonizing antibodies.[46] The comparative release profiles of soluble particles versus hydrogels may help to determine whether CPMV-based vaccines are inherently Th1-mediated adjuvants or whether the nature of the epitope is the main determinant of Th1/2 bias.

Vaccine efficacy and safety are important design parameters, and while Th2 bias is desired to elicit neutralizing IgG1 antibodies for humoral protection against viruses prior to cell entry and establishment of infection, reports highlight the risk of antibody-dependent enhancement (ADE) with the SARS and Middle East Respiratory Syndrome coronavirus vaccine candidates.[83,84] Some reports suspected similar risk of ADE for SARS-CoV-2 vaccines;[85,86] nevertheless, the rationale design and choice of target epitope may provide greater safety compared to subunit vaccines containing RBD or the full-length S protein.

CONCLUSIONS

We have formulated an injectable hydrogel containing CPMV conjugated to B-cell epitope 826 as a single-dose vaccine candidate for COVID-19. CPMV hydrogel formulations were prepared using chitosan and GP solutions to yield a liquid mixture that was homogenized with CPMV particles at room temperature. HMW chitosan formulations (F3) containing 0−4.5 mg mL^{-1} CPMV achieved a relatively fast transition from liquid solutions to gels at 37 °C (gelation time 5−8 min) and slowly released Cy5-CPMV particles in vitro and in vivo. Most importantly, F3 containing CPMV labeled with epitope 826 from the SARS-CoV-2 S protein induced high antibody titers over 20 weeks, with an associated shift from Th1-biased to Th2-biased profiles. Our findings suggest that CPMV nanoparticles can be effectively formulated in chitosan/GP hydrogels and are released over several months as intact and biologically active particles with conserved immunotherapeutic efficacy. The proposed formulation not only represents a promising single-dose vaccine candidate to address future pandemics but may also facilitate the development of long-lasting plant virus-based nanomedicines for diseases that require long-term treatment.

ASSOCIATED CONTENT

Supporting Information

The Supporting Information is available free of charge at https://pubs.acs.org/doi/10.1021/acs.biomac.2c00112.

Formulation gelation times; SEM images of hydrogels; agarose and SDS-PAGE gels of Cy5-CPMV released; and mutations in SARS-CoV-2 variants (PDF)

AUTHOR INFORMATION

Corresponding Author

Nicole F. Steinmetz − *Department of NanoEngineering, University of California San Diego, La Jolla, California*

https://doi.org/10.1021/acs.biomac.2c00112
Biomacromolecules 2022, 23, 1812−1825

92039, United States; Department of Bioengineering, Department of Radiology, Center for Nano-ImmunoEngineering, Moores Cancer Center, and Institute for Materials Discovery and Design, University of California San Diego, La Jolla, California 92039, United States; orcid.org/0000-0002-0130-0481; Email: nsteinmetz@ucsd.edu

Authors

Christian Isalomboto Nkanga − *Department of NanoEngineering, University of California San Diego, La Jolla, California 92039, United States*

Oscar A. Ortega-Rivera − *Department of NanoEngineering, University of California San Diego, La Jolla, California 92039, United States; Center for Nano-ImmunoEngineering, University of California San Diego, La Jolla, California 92039, United States;* orcid.org/0000-0002-0773-0677

Matthew D. Shin − *Department of NanoEngineering, University of California San Diego, La Jolla, California 92039, United States; Center for Nano-ImmunoEngineering, University of California San Diego, La Jolla, California 92039, United States*

Miguel A. Moreno-Gonzalez − *Department of NanoEngineering, University of California San Diego, La Jolla, California 92039, United States; Center for Nano-ImmunoEngineering, University of California San Diego, La Jolla, California 92039, United States;* orcid.org/0000-0002-1601-9369

Complete contact information is available at: https://pubs.acs.org/10.1021/acs.biomac.2c00112

Notes

The authors declare the following competing financial interest(s): Dr. Steinmetz is a co-founder of, has equity in, and has a financial interest with Mosaic ImmunoEngineering Inc. Dr. Steinmetz serves as Director, Board Member, and Acting Chief Scientific Officer, and paid consultant to Mosaic. The other authors declare no potential conflicts of interest.

■ ACKNOWLEDGMENTS

This work was supported by the NSF Center for the Chemistry of Molecularly Optimized Networks (MONET), CHE-2116298. Animal studies were supported by start-up funds to N.F.S. O.A.O.-R. acknowledges a UC MEXUS-CONACYT Postdoctoral Fellowship, FE-20-136. The authors thank Dr. Soo Khim Chan (UC San Diego) for technical assistance with TEM imaging and Dr. Sourabh Shukla and Young Hun Chung (UC San Diego) for assistance with animal studies.

■ REFERENCES

(1) Zhu, N.; Zhang, D.; Wang, W.; Li, X.; Yang, B.; Song, J.; Zhao, X.; Huang, B.; Shi, W.; Lu, R.; Niu, P.; Zhan, F.; Ma, X.; Wang, D.; Xu, W.; Wu, G.; Gao, G. F.; Tan, W. A Novel Coronavirus from Patients with Pneumonia in China, 2019. *N. Engl. J. Med.* **2020**, *382*, 727−733.

(2) World Health Organization. The True Death Toll of COVID-19. Https://Www.Who.Int/Data/Stories/the-True-Death-Toll-of-Covid-19-Estimating-Global-Excess-Mortality (Last accessed Dec 1 2021).

(3) Statista. Number of Cumulative Cases of Coronavirus (COVID-19) Worldwide from January 22, 2020 to November 22, 2021. Https://Www.Statista.Com/Statistics/1103040/Cumulative-Coronavirus-Covid19-Cases-Number-Worldwide-by-Day/byDay (Last accessed on Dec 1, 2020).

(4) Polack, F. P.; Thomas, S. J.; Kitchin, N.; Absalon, J.; Gurtman, A.; Lockhart, S.; Perez, J. L.; Pérez Marc, G.; Moreira, E. D.; Zerbini, C.; Bailey, R.; Swanson, K. A.; Roychoudhury, S.; Koury, K.; Li, P.; Kalina, W. V.; Cooper, D.; Frenck, R. W.; Hammitt, L. L.; Türeci, Ö.; Nell, H.; Schaefer, A.; Ünal, S.; Tresnan, D. B.; Mather, S.; Dormitzer, P. R.; Şahin, U.; Jansen, K. U.; Gruber, W. C. Safety and Efficacy of the BNT162b2 MRNA Covid-19 Vaccine. *N. Engl. J. Med.* **2020**, *383*, 2603−2615.

(5) Voysey, M.; Clemens, S. A. C.; Madhi, S. A.; Weckx, L. Y.; Folegatti, P. M.; Aley, P. K.; Angus, B.; Baillie, V. L.; Baillie, S. L.; Bhorat, Q. E.; Bibi, S.; Briner, C.; Cicconi, P.; Collins, A. M.; Colin-Jones, R.; Cutland, C. L.; Darton, T. C.; Dheda, K.; Duncan, C. J. A.; Emary, K. R. W.; Ewer, K. J.; Fairlie, L.; Faust, S. N.; Feng, S.; Ferreira, D. M.; Finn, A.; Goodman, A. L.; Green, C. M.; Green, C. A.; Heath, P. T.; Hill, C.; Hill, H.; Hirsch, I.; Hodgson, S. H. C.; Izu, A.; Jackson, S.; Jenkin, D.; Joe, C. C. D.; Kerridge, S.; Koen, A.; Kwatra, G.; Lazarus, R.; Lawrie, A. M.; Lelliott, A.; Libri, V.; Lillie, P. J.; Mallory, R.; Mendes, A. V. A.; Milan, E. P.; Minassian, A. M.; McGregor, A.; Morrison, H.; Mujadidi, Y. F.; Nana, A.; O'Reilly, P. J.; Padayachee, S. D.; Pittella, A.; Plested, E.; Pollock, K. M.; Ramasamy, M. N.; Rhead, S.; Schwarzbold, A. V.; Singh, N.; Smith, A.; Song, R.; Snape, M. D.; Sprinz, E.; Sutherland, R. K.; Tarrant, R.; Thomson, E. C.; Török, M. E.; Toshner, M.; Turner, D. P. J.; Vekemans, J.; Villafana, T. L.; Watson, M. E. E.; Williams, C. J.; Douglas, A. D.; Hill, A. V. S.; Lambe, T.; Gilbert, S. C.; Pollard, A. J. on behalf of the O. C. V. T. G. Safety and Efficacy of the ChAdOx1 NCoV-19 Vaccine (AZD1222) against SARS-CoV-2: An Interim Analysis of Four Randomised Controlled Trials in Brazil, South Africa, and the UK. *Lancet* **2021**, *397*, 99−111.

(6) GOV.UK. Moderna COVID-19 Vaccine Authorised by UK Medicines Regulator. Jan 8, 2021. Https://Www.Gov.Uk/Government/News/Moderna-Covid-19-Vaccine-Authorised-by-Uk-Medicines-Regulator (accessed Dec 30, 2021).

(7) World Health Organization. WHO Coronavirus (COVID-19) Dashboard. Https://Covid19.Who.Int/ (Last accessed Dec 30, 2021).

(8) Moore, S.; Hill, E. M.; Tildesley, M. J.; Dyson, L.; Keeling, M. J. Vaccination and Non-Pharmaceutical Interventions for COVID-19: A Mathematical Modelling Study. *Lancet Infect. Dis.* **2021**, *21*, 793−802.

(9) Chung, Y. H.; Church, D.; Koellhoffer, E. C.; Osota, E.; Shukla, S.; Rybicki, E. P.; Pokorski, J. K.; Steinmetz, N. F. Integrating Plant Molecular Farming and Materials Research for Next-Generation Vaccines. *Nat. Rev. Mater.* **2021**, DOI: 10.1038/s41578-021-00399-5.

(10) Matrajt, L.; Eaton, J.; Leung, T.; Dimitrov, D.; Schiffer, J. T.; Swan, D. A.; Janes, H. Optimizing Vaccine Allocation for COVID-19 Vaccines Shows the Potential Role of Single-Dose Vaccination. *Nat. Commun.* **2021**, *12*, 1−18.

(11) Tuite, A. R.; Zhu, L.; Fisman, D. N.; Salomon, J. A. Alternative Dose Allocation Strategies to Increase Benefits From Constrained COVID-19 Vaccine Supply. *Ann. Intern. Med.* **2021**, *174*, 570−572.

(12) Barnabas, R. V.; Wald, A. A Public Health COVID-19 Vaccination Strategy to Maximize the Health Gains for Every Single Vaccine Dose. *Ann. Intern. Med.* **2021**, *174*, 552−553.

(13) Paltiel, A. D.; Zheng, A.; Schwartz, J. L. Speed versus Efficacy: Quantifying Potential Tradeoffs in COVID-19 Vaccine Deployment. *Ann. Intern. Med.* **2021**, *174*, 568−570.

(14) Sabino, E. C.; Buss, L. F.; Carvalho, M. P. S.; Prete, C. A.; Crispim, M. A. E.; Fraiji, N. A.; Pereira, R. H. M.; Parag, K. V.; da Silva Peixoto, P.; Kraemer, M. U. G.; Oikawa, M. K.; Salomon, T.; Cucunuba, Z. M.; Castro, M. C.; de Souza Santos, A. A.; Nascimento, V. H.; Pereira, H. S.; Ferguson, N. M.; Pybus, O. G.; Kucharski, A.; Busch, M. P.; Dye, C.; Faria, N. R. Resurgence of COVID-19 in Manaus, Brazil, despite High Seroprevalence. *Lancet* **2021**, *397*, 452−455.

(15) Davies, N. G.; Abbott, S.; Barnard, R. C.; Jarvis, C. I.; Kucharski, A. J.; Munday, J. D.; Pearson, C. A. B.; Russell, T. W.; Tully, D. C.; Washburne, A. D.; Wenseleers, T.; Gimma, A.; Waites, W.; Wong, K. L. M.; van Zandvoort, K.; Silverman, J. D.; Diaz-Ordaz, K.; Keogh, R.; Eggo, R. M.; Funk, S.; Jit, M.; Atkins, K. E.; Edmunds,

W. J. Estimated Transmissibility and Impact of SARS-CoV-2 Lineage B.1.1.7 in England. *Science 80-* **2021**, *372*, 372.
(16) Callaway, E. DELTA CORONAVIRUS VARIANT: SCIENTISTS BRACE FOR IMPACT. *Nature* **2021**, *595*, 17−18.
(17) Challen, R.; Brooks-Pollock, E.; Read, J. M.; Dyson, L.; Tsaneva-Atanasova, K.; Danon, L. Risk of Mortality in Patients Infected with SARS-CoV-2 Variant of Concern 202012/1: Matched Cohort Study. *BMJ* **2021**, *372*, n579.
(18) Chen, Y.; Zuiani, A.; Fischinger, S.; Mullur, J.; Atyeo, C.; Travers, M.; Lelis, F. J. N.; Pullen, K. M.; Martin, H.; Tong, P.; Gautam, A.; Habibi, S.; Bensko, J.; Gakpo, D.; Feldman, J.; Hauser, B. M.; Caradonna, T. M.; Cai, Y.; Burke, J. S.; Lin, J.; Lederer, J. A.; Lam, E. C.; Lavine, C. L.; Seaman, M. S.; Chen, B.; Schmidt, A. G.; Balazs, A. B.; Lauffenburger, D. A.; Alter, G.; Wesemann, D. R. Quick COVID-19 Healers Sustain Anti-SARS-CoV-2 Antibody Production. *Cell* **2020**, *183*, 1496−1507 e16.
(19) Roberto, B.; Topol, E. J. Assessing the Human Immune Response to SARS-CoV-2 Variants. *Nat. Med.* **2021**, *27*, 571−572.
(20) Wang, Z.; Schmidt, F.; Weisblum, Y.; Muecksch, F.; Barnes, C. O.; Finkin, S.; Schaefer-Babajew, D.; Cipolla, M.; Gaebler, C.; Lieberman, J. A.; Oliveira, T. Y.; Yang, Z.; Abernathy, M. E.; Huey-Tubman, K. E.; Hurley, A.; Turroja, M.; West, K. A.; Gordon, K.; Millard, K. G.; Ramos, V.; Da Silva, J.; Xu, J.; Colbert, R. A.; Patel, R.; Dizon, J.; Unson-O'Brien, C.; Shimeliovich, I.; Gazumyan, A.; Caskey, M.; Bjorkman, P. J.; Casellas, R.; Hatziioannou, T.; Bieniasz, P. D.; Nussenzweig, M. C. MRNA Vaccine-Elicited Antibodies to SARS-CoV-2 and Circulating Variants. *Nature* **2021**, *592*, 616−622.
(21) Li, Q.; Nie, J.; Wu, J.; Zhang, L.; Ding, R.; Wang, H.; Zhang, Y.; Li, T.; Liu, S.; Zhang, M.; Zhao, C.; Liu, H.; Nie, L.; Qin, H.; Wang, M.; Lu, Q.; Li, X.; Liu, J.; Liang, H.; Shi, Y.; Shen, Y.; Xie, L.; Zhang, L.; Qu, X.; Xu, W.; Huang, W.; Wang, Y. SARS-CoV-2 501Y.V2 Variants Lack Higher Infectivity but Do Have Immune Escape. *Cell* **2021**, *184*, 2362−2371 e9.
(22) London School of Hygiene & Tropical Medicine. (2021) COVID-19 Vaccine Tracker. Https://Vac-Lshtm.Shinyapps.Io/Ncov_vaccine_landscape/ (accessed on Dec 30, 2021).
(23) Zhang, Y.-N.; Paynter, J.; Sou, C.; Fourfouris, T.; Wang, Y.; Abraham, C.; Ngo, T.; Zhang, Y.; He, L.; Zhu, J. Mechanism of a COVID-19 Nanoparticle Vaccine Candidate That Elicits a Broadly Neutralizing Antibody Response to SARS-CoV-2 Variants. *Sci. Adv.* **2021**, *7*, 1−21.
(24) Williams, T. C.; Burgers, W. A. SARS-CoV-2 Evolution and Vaccines: Cause for Concern? *Lancet Respir. Med.* **2021**, *9*, 333−335.
(25) Logunov, D. Y.; Dolzhikova, I. V.; Shcheblyakov, D. V.; Tukhvatulin, A. I.; Zubkova, O. V.; Dzharullaeva, A. S.; Kovyrshina, A. V.; Lubenets, N. L.; Grousova, D. M.; Erokhova, A. S.; Botikov, A. G.; Izhaeva, F. M.; Popova, O.; Ozharovskaya, T. A.; Esmagambetov, I. B.; Favorskaya, I. A.; Zrelkin, D. I.; Voronina, D. V.; Shcherbinin, D. N.; Semikhin, A. S.; Simakova, Y. V.; Tokarskaya, E. A.; Egorova, D. A.; Shmarov, M. M.; Nikitenko, N. A.; Gushchin, V. A.; Smolyarchuk, E. A.; Zyryanov, S. K.; Borisevich, S. V.; Naroditsky, B. S.; Gintsburg, A. L. Safety and Efficacy of an RAd26 and RAd5 Vector-Based Heterologous Prime-Boost COVID-19 Vaccine: An Interim Analysis of a Randomised Controlled Phase 3 Trial in Russia. *Lancet* **2021**, *397*, 671−681.
(26) Heath, P. T.; Galiza, E. P.; Baxter, D. N.; Boffito, M.; Browne, D.; Burns, F.; Chadwick, D. R.; Clark, R.; Cosgrove, C.; Galloway, J.; Goodman, A. L.; Heer, A.; Higham, A.; Iyengar, S.; Jamal, A.; Jeanes, C.; Kalra, P. A.; Kyriakidou, C.; McAuley, D. F.; Meyrick, A.; Minassian, A. M.; Minton, J.; Moore, P.; Munsoor, I.; Nicholls, H.; Osanlou, O.; Packham, J.; Pretswell, C. H.; San Francisco Ramos, A.; Saralaya, D.; Sheridan, R. P.; Smith, R.; Soiza, R. L.; Swift, P. A.; Thomson, E. C.; Turner, J.; Viljoen, M. E.; Albert, G.; Cho, I.; Dubovsky, F.; Glenn, G.; Rivers, J.; Robertson, A.; Smith, K.; Toback, S. Safety and Efficacy of NVX-CoV2373 Covid-19 Vaccine. *N. Engl. J. Med.* **2021**, *385*, 1172−1183.
(27) Thompson, M. G.; Burgess, J. L.; Naleway, A. L.; Tyner, H.; Yoon, S. K.; Meece, J.; Olsho, L. E. W.; Caban-Martinez, A. J.; Fowlkes, A. L.; Lutrick, K.; Groom, H. C.; Dunnigan, K.; Odean, M. J.; Hegmann, K.; Stefanski, E.; Edwards, L. J.; Schaefer-Solle, N.; Grant, L.; Ellingson, K.; Kuntz, J. L.; Zunie, T.; Thiese, M. S.; Ivacic, L.; Wesley, M. G.; Mayo Lamberte, J.; Sun, X.; Smith, M. E.; Phillips, A. L.; Groover, K. D.; Yoo, Y. M.; Gerald, J.; Brown, R. T.; Herring, M. K.; Joseph, G.; Beitel, S.; Morrill, T. C.; Mak, J.; Rivers, P.; Poe, B. P.; Lynch, B.; Zhou, Y.; Zhang, J.; Kelleher, A.; Li, Y.; Dickerson, M.; Hanson, E.; Guenther, K.; Tong, S.; Bateman, A.; Reisdorf, E.; Barnes, J.; Azziz-Baumgartner, E.; Hunt, D. R.; Arvay, M. L.; Kutty, P.; Fry, A. M.; Gaglani, M. Prevention and Attenuation of Covid-19 with the BNT162b2 and MRNA-1273 Vaccines. *N. Engl. J. Med.* **2021**, *385*, 320−329.
(28) Baden, L. R.; El Sahly, H. M.; Essink, B.; Kotloff, K.; Frey, S.; Novak, R.; Diemert, D.; Spector, S. A.; Rouphael, N.; Creech, C. B.; McGettigan, J.; Khetan, S.; Segall, N.; Solis, J.; Brosz, A.; Fierro, C.; Schwartz, H.; Neuzil, K.; Corey, L.; Gilbert, P.; Janes, H.; Follmann, D.; Marovich, M.; Mascola, J.; Polakowski, L.; Ledgerwood, J.; Graham, B. S.; Bennett, H.; Pajon, R.; Knightly, C.; Leav, B.; Deng, W.; Zhou, H.; Han, S.; Ivarsson, M.; Miller, J.; Zaks, T. Efficacy and Safety of the MRNA-1273 SARS-CoV-2 Vaccine. *N. Engl. J. Med.* **2021**, *384*, 403−416.
(29) Lupala, C. S.; Kumar, V.; Su, X.-d.; Wu, C.; Liu, H. Computational Insights into Differential Interaction of Mammalian Angiotensin-Converting Enzyme 2 with the SARS-CoV-2 Spike Receptor Binding Domain. *Comput. Biol. Med.* **2022**, *141*, 105017.
(30) Garcia-Beltran, W. F.; Lam, E. C.; St. Denis, K.; Nitido, A. D.; Garcia, Z. H.; Hauser, B. M.; Feldman, J.; Pavlovic, M. N.; Gregory, D. J.; Poznansky, M. C.; Sigal, A.; Schmidt, A. G.; Iafrate, A. J.; Naranbhai, V.; Balazs, A. B. Multiple SARS-CoV-2 Variants Escape Neutralization by Vaccine-Induced Humoral Immunity. *Cell* **2021**, *184*, 2523.
(31) Wang, P.; Nair, M. S.; Liu, L.; Iketani, S.; Luo, Y.; Guo, Y.; Wang, M.; Yu, J.; Zhang, B.; Kwong, P. D.; Graham, B. S.; Mascola, J. R.; Chang, J. Y.; Yin, M. T.; Sobieszczyk, M.; Kyratsous, C. A.; Shapiro, L.; Sheng, Z.; Huang, Y.; Ho, D. D. Antibody Resistance of SARS-CoV-2 Variants B.1.351 and B.1.1.7. *Nature* **2021**, *593*, 130−135.
(32) Andreano, E.; Piccini, G.; Licastro, D.; Casalino, L.; Johnson, N. V.; Paciello, I.; Dal Monego, S.; Pantano, E.; Manganaro, N.; Manenti, A.; Manna, R.; Casa, E.; Hyseni, I.; Benincasa, L.; Montomoli, E.; Amaro, R. E.; McLellan, J. S.; Rappuoli, R. SARS-CoV-2 Escape from a Highly Neutralizing COVID-19 Convalescent Plasma. *Proc. Natl. Acad. Sci. U.S.A.* **2021**, *118*, 1−7.
(33) Wibmer, C. K.; Ayres, F.; Hermanus, T.; Madzivhandila, M.; Kgagudi, P.; Oosthuysen, B.; Lambson, B. E.; de Oliveira, T.; Vermeulen, M.; van der Berg, K.; Rossouw, T.; Boswell, M.; Ueckermann, V.; Meiring, S.; von Gottberg, A.; Cohen, C.; Morris, L.; Bhiman, J. N.; Moore, P. L. SARS-CoV-2 501Y.V2 Escapes Neutralization by South African COVID-19 Donor Plasma. *Nat. Med.* **2021**, *27*, 622−625.
(34) Cherian, S.; Potdar, V.; Jadhav, S.; Yadav, P.; Gupta, N.; Das, M.; Rakshit, P.; Singh, S.; Abraham, P.; Panda, S.; Team, N. I. C. SARS-CoV-2 Spike Mutations, L452R, T478K, E484Q and P681R, in the Second Wave of COVID-19 in Maharashtra, India. *Microorganism* **2021**, *9*, 1542.
(35) Tegally, H.; Wilkinson, E.; Giovanetti, M.; Iranzadeh, A.; Fonseca, V.; Giandhari, J.; Doolabh, D.; Pillay, S.; San, E. J.; Msomi, N.; Mlisana, K.; von Gottberg, A.; Walaza, S.; Allam, M.; Ismail, A.; Mohale, T.; Glass, A. J.; Engelbrecht, S.; Van Zyl, G.; Preiser, W.; Petruccione, F.; Sigal, A.; Hardie, D.; Marais, G.; Hsiao, N.-y.; Korsman, S.; Davies, M.-A.; Tyers, L.; Mudau, I.; York, D.; Maslo, C.; Goedhals, D.; Abrahams, S.; Laguda-Akingba, O.; Alisoltani-Dehkordi, A.; Godzik, A.; Wibmer, C. K.; Sewell, B. T.; Lourenço, J.; Alcantara, L. C. J.; Kosakovsky Pond, S. L.; Weaver, S.; Martin, D.; Lessells, R. J.; Bhiman, J. N.; Williamson, C.; de Oliveira, T. Detection of a SARS-CoV-2 Variant of Concern in South Africa. *Nature* **2021**, *592*, 438−443.
(36) Li, Q.; Wu, J.; Nie, J.; Zhang, L.; Hao, H.; Liu, S.; Zhao, C.; Zhang, Q.; Liu, H.; Nie, L.; Qin, H.; Wang, M.; Lu, Q.; Li, X.; Sun, Q.; Liu, J.; Zhang, L.; Li, X.; Huang, W.; Wang, Y. The Impact of

https://doi.org/10.1021/acs.biomac.2c00112
Biomacromolecules 2022, 23, 1812−1825

Mutations in SARS-CoV-2 Spike on Viral Infectivity and Antigenicity. *Cell* **2020**, *182*, 1284−1294 e9.
(37) Rees-Spear, C.; Muir, L.; Griffith, S. A.; Heaney, J.; Aldon, Y.; Snitselaar, J. L.; Thomas, P.; Graham, C.; Seow, J.; Lee, N.; Rosa, A.; Roustan, C.; Houlihan, C. F.; Sanders, R. W.; Gupta, R. K.; Cherepanov, P.; Stauss, H. J.; Nastouli, E.; Doores, K. J.; van Gils, M. J.; McCoy, L. E. The Effect of Spike Mutations on SARS-CoV-2 Neutralization. *Cell Rep.* **2021**, *34*, 108890.
(38) Jiang, S.; Hillyer, C.; Du, L. Neutralizing Antibodies against SARS-CoV-2 and Other Human Coronaviruses. *Trends Immunol.* **2020**, *41*, 355−359.
(39) Ortega-Rivera, O. A.; Shin, M. D.; Chen, A.; Beiss, V.; Moreno-Gonzalez, M. A.; Lopez-Ramirez, M. A.; Reynoso, M.; Wang, H.; Hurst, B. L.; Wang, J.; Pokorski, J. K.; Steinmetz, N. F. Trivalent Subunit Vaccine Candidates for COVID-19 and Their Delivery Devices. *J. Am. Chem. Soc.* **2021**, *143*, 14748−14765.
(40) Bachmann, M. F.; Jennings, G. T. Vaccine Delivery: A Matter of Size, Geometry, Kinetics and Molecular Patterns. *Nat. Rev. Immunol.* **2010**, *10*, 787−796.
(41) Shukla, S.; Myers, J. T.; Woods, S. E.; Gong, X.; Czapar, A. E.; Commandeur, U.; Huang, A. Y.; Levine, A. D.; Steinmetz, N. F. Plant Viral Nanoparticles-Based HER2 Vaccine: Immune Response Influenced by Differential Transport, Localization and Cellular Interactions of Particulate Carriers. *Biomaterials* **20172017**, *121*, 15−27.
(42) Huynh, N. T.; Hesketh, E. L.; Saxena, P.; Meshcheriakova, Y.; Ku, Y.-C.; Hoang, L. T.; Johnson, J. E.; Ranson, N. A.; Lomonossoff, G. P.; Reddy, V. S. Crystal Structure and Proteomics Analysis of Empty Virus-like Particles of Cowpea Mosaic Virus. *Structure* **2016**, *24*, 567−575.
(43) Ortega-Rivera, O. A.; Shukla, S.; Shin, M. D.; Chen, A.; Beiss, V.; Moreno-Gonzalez, M. A.; Zheng, Y.; Clark, A. E.; Carlin, A. F.; Pokorski, J. K.; Steinmetz, N. F. Cowpea Mosaic Virus Nanoparticle Vaccine Candidates Displaying Peptide Epitopes Can Neutralize the Severe Acute Respiratory Syndrome Coronavirus. *ACS Infect. Dis.* **2021**, *7*, 3096−3110.
(44) Wang, C.; Beiss, V.; Steinmetz, N. F. Cowpea Mosaic Virus Nanoparticles and Empty Virus-Like Particles Show Distinct but Overlapping Immunostimulatory Properties. *J. Virol.* **2019**, *93*, No. e00129-19.
(45) Murray, A. A.; Wang, C.; Fiering, S.; Steinmetz, N. F. In Situ Vaccination with Cowpea vs Tobacco Mosaic Virus against Melanoma. *Mol. Pharm.* **2018**, *15*, 3700−3716.
(46) Shukla, S.; Wang, C.; Beiss, V.; Steinmetz, N. F. Antibody Response against Cowpea Mosaic Viral Nanoparticles Improves in Situ Vaccine Efficacy in Ovarian Cancer. *ACS Nano* **2020**, *14*, 2994−3003.
(47) Lizotte, P. H.; Wen, A. M.; Sheen, M. R.; Fields, J.; Rojanasopondist, P.; Steinmetz, N. F.; Fiering, S. In Situ Vaccination with Cowpea Mosaic Virus Nanoparticles Suppresses Metastatic Cancer. *Nat. Nanotechnol.* **2015**, *11*, 295−303.
(48) Hoopes, P. J.; Wagner, R. J.; Duval, K.; Kang, K.; Gladstone, D. J.; Moodie, K. L.; Crary-Burney, M.; Ariaspulido, H.; Veliz, F. A.; Steinmetz, N. F.; Fiering, S. N. Treatment of Canine Oral Melanoma with Nanotechnology-Based Immunotherapy and Radiation. *Mol. Pharm.* **2018**, *15*, 3717−3722.
(49) Zheng, Y.; Lee, P. W.; Wang, C.; Thomas, L. D.; Stewart, P. L.; Steinmetz, N. F.; Pokorski, J. K. Freeze-Drying to Produce Efficacious CPMV Virus-like Particles. *Nano Lett.* **2019**, *19*, 2099−2105.
(50) Dash, M.; Chiellini, F.; Ottenbrite, R. M.; Chiellini, E. Chitosan-A versatile semi-synthetic polymer in biomedical applications. *Prog. Polym. Sci.* **2011**, *36*, 981−1014.
(51) Lehr, C.-M.; Bouwstra, J. A.; Schacht, E. H.; Junginger, H. E. In Vitro Evaluation of Mucoadhesive Properties of Chitosan and Some Other Natural Polymers. *Int. J. Pharm.* **1992**, *78*, 43−48.
(52) SmithNephew. CarGel BioScaffold Https://Www.Smith-Nephew.Com/Key-Products/Sports-Medicine/Bst-Cargel/ (accessed on Dec 03, 2021.
(53) Illum, L.; Jabbal-Gill, I.; Hinchcliffe, M.; Fisher, A. N.; Davis, S. S. Chitosan as a Novel Nasal Delivery System for Vaccines. *Adv. Drug Deliv. Rev.* **2001**, *51*, 81−96.
(54) Ghendon, Y.; Markushin, S.; Krivtsov, G.; Akopova, I. Chitosan as an Adjuvant for Parenterally Administered Inactivated Influenza Vaccines. *Arch. Virol.* **2008**, *153*, 831−837.
(55) Scherließ, R.; Buske, S.; Young, K.; Weber, B.; Rades, T.; Hook, S. In vivo evaluation of chitosan as an adjuvant in subcutaneous vaccine formulations. *Vaccine* **2013**, *31*, 4812−4819.
(56) Chenite, A.; Buschmann, M.; Wang, D.; Chaput, C.; Kandani, N. Rheological Characterisation of Thermogelling Chitosan/Glycerol-Phosphate Solutions. *Carbohydr. Polym.* **2001**, *46*, 39−47.
(57) Cho, J.; Heuzey, M.-C.; Bégin, A.; Carreau, P. J. Physical Gelation of Chitosan in the Presence of β-Glycerophosphate: The Effect of Temperature. *Biomacromolecules* **2005**, *6*, 3267−3275.
(58) Zhou, H. Y.; Jiang, L. J.; Cao, P. P.; Li, J. B.; Chen, X. G. Glycerophosphate-Based Chitosan Thermosensitive Hydrogels and Their Biomedical Applications. *Carbohydr. Polym.* **2015**, *117*, 524−536.
(59) Rafael, D.; Melendres, M. M. R.; Andrade, F.; Montero, S.; Martinez-Trucharte, F.; Vilar-Hernandez, M.; Durán-Lara, E. F.; Schwartz Jr, S.; Abasolo, I. Thermo-Responsive Hydrogels for Cancer Local Therapy: Challenges and State-of-Art. *Int. J. Pharm.* **2021**, *606*, 120954.
(60) Rahmanian-Devin, P.; Baradaran Rahimi, V.; Askari, V. R. Thermosensitive Chitosan-β-Glycerophosphate Hydrogels as Targeted Drug Delivery Systems: An Overview on Preparation and Their Applications. *Adv. Pharmacol. Pharm. Sci.* **2021**, *2021*, 1.
(61) Al Sabbagh, C.; Seguin, J.; Agapova, E.; Kramerich, D.; Boudy, V.; Mignet, N. Thermosensitive Hydrogels for Local Delivery of 5-Fluorouracil as Neoadjuvant or Adjuvant Therapy in Colorectal Cancer. *Eur. J. Pharm. Biopharm.* **2020**, *157*, 154−164.
(62) Mei, E.; Chen, C.; Li, C.; Ding, X.; Chen, J.; Xi, Q.; Zhou, S.; Liu, J.; Li, Z. Injectable and Biodegradable Chitosan Hydrogel-Based Drug Depot Contributes to Synergistic Treatment of Tumors. *Biomacromolecules* **2021**, *22*, 5339−5348.
(63) Song, K.; Li, l.; Yan, X.; Zhang, W.; Zhang, Y.; Wang, Y.; Liu, T. Characterization of human adipose tissue-derived stem cells in vitro culture and in vivo differentiation in a temperature-sensitive chitosan/β- glycerophosphate/collagen hybrid hydrogel. *Mater. Sci. Eng., C* **2017**, *70*, 231−240.
(64) Stanzione, A.; Polini, A.; La Pesa, V.; Quattrini, A.; Romano, A.; Gigli, G.; Moroni, L.; Gervaso, F. Thermosensitive Chitosan-Based Hydrogels Supporting Motor Neuron-like NSC-34 Cell Differentiation. *Biomater. Sci.* **2021**, *9*, 7492−7503.
(65) Peng, Q.; Sun, X.; Gong, T.; Wu, C.-Y.; Zhang, T.; Tan, J.; Zhang, Z.-R. Injectable and Biodegradable Thermosensitive Hydrogels Loaded with PHBHHx Nanoparticles for the Sustained and Controlled Release of Insulin. *Acta Biomater.* **2013**, *9*, 5063−5069.
(66) Li, X.; Zheng, X.; Wei, X.; Guo, G.; Gou, M.; Gong, C.; Wang, X.; Dai, M.; Chen, L.; Wei, Y.; Qian, Z. A Novel Composite Drug Delivery System: Honokiol Nanoparticles in Thermosensitive Hydrogel Based on Chitosan. *J. Nanosci. Nanotechnol.* **2009**, *9*, 4586−4592.
(67) Wen, A. M.; Shukla, S.; Saxena, P.; Aljabali, A. A. A.; Yildiz, I.; Dey, S.; Mealy, J. E.; Yang, A. C.; Evans, D. J.; Lomonossoff, G. P.; Steinmetz, N. F. Interior Engineering of a Viral Nanoparticle and Its Tumor Homing Properties. *Biomacromolecules* **2012**, *13*, 3990−4001.
(68) Wen, A. M.; Lee, K. L.; Yildiz, I.; Bruckman, M. A.; Shukla, S.; Steinmetz, N. F. Viral Nanoparticles for in Vivo Tumor Imaging. *J. Visualized Exp.* **20122012**, *69*, No. e4352.
(69) Shin, M. D.; Hochberg, J. D.; Pokorski, J. K.; Steinmetz, N. F. Bioconjugation of Active Ingredients to Plant Viral Nanoparticles Is Enhanced by Preincubation with a Pluronic F127 Polymer Scaffold. *ACS Appl. Mater. Interfaces* **2021**, *13*, 59618−59632.
(70) Zhou, P.; Li, X.; Zhang, B.; Shi, Q.; Li, D.; Ju, X. A Human Umbilical Cord Mesenchymal Stem Cell-Conditioned Medium/Chitosan/Collagen/β-Glycerophosphate Thermosensitive Hydrogel Promotes Burn Injury Healing in Mice. *BioMed Res. Int.* **2019**, *2019*, 1.

https://doi.org/10.1021/acs.biomac.2c00112
Biomacromolecules 2022, 23, 1812−1825

(71) Wen, A. M.; Infusino, M.; De Luca, A.; Kernan, D. L.; Czapar, A. E.; Strangi, G.; Steinmetz, N. F. Interface of Physics and Biology: Engineering Virus-Based Nanoparticles for Biophotonics. *Bioconjugate Chem.* **2015**, *26*, 51−62.
(72) Chenite, A.; Chaput, C.; Wang, D.; Combes, C.; Buschmann, M. D.; Hoemann, C. D.; Leroux, J. C.; Atkinson, B. L.; Binette, F.; Selmani, A. Novel Injectable Neutral Solutions of Chitosan Form Biodegradable Gels in Situ. *Biomaterials* **2000**, *21*, 2155−2161.
(73) Liu, P.; Li, M.; Yu, H.; Fang, H.; Yin, J.; Zhu, D.; Yang, Q.; Ke, Q.; Huang, Y.; Guo, Y.; Gao, Y.; Zhang, C. Biphasic CK2.1-coated β-glycerophosphate chitosan/LL37-modified layered double hydroxide chitosan composite scaffolds enhance coordinated hyaline cartilage and subchondral bone regeneration. *Chem. Eng. J.* **2021**, *418*, 129531.
(74) Aliaghaie, M.; Mirzadeh, H.; Dashtimoghadam, E.; Taranejoo, S. Investigation of Gelation Mechanism of an Injectable Hydrogel Based on Chitosan by Rheological Measurements for a Drug Delivery Application. *Soft Matter* **2012**, *8*, 7128−7137.
(75) Teles, H.; Vermonden, T.; Eggink, G.; Hennink, W. E.; de Wolf, F. A. Hydrogels of Collagen-Inspired Telechelic Triblock Copolymers for the Sustained Release of Proteins. *J. Controlled Release* **2010**, *147*, 298−303.
(76) Ukmar, T.; Maver, U.; Planinšek, O.; Kaučič, V.; Gaberšček, M.; Godec, A. Understanding Controlled Drug Release from Mesoporous Silicates: Theory and Experiment. *J. Controlled Release* **2011**, *155*, 409−417.
(77) Ukmar, T.; Gaberšček, M.; Merzel, F.; Godec, A. Modus Operandi of Controlled Release from Mesoporous Matrices: A Theoretical Perspective. *Phys. Chem. Chem. Phys.* **2011**, *13*, 15311−15317.
(78) Czapar, A. E.; Tiu, B. D. B.; Veliz, F. A.; Pokorski, J. K.; Steinmetz, N. F. Slow-Release Formulation of Cowpea Mosaic Virus for In Situ Vaccine Delivery to Treat Ovarian Cancer. *Adv. Sci.* **2018**, *5*, 1700991.
(79) Cai, H.; Shukla, S.; Wang, C.; Masarapu, H.; Steinmetz, N. F. Heterologous Prime-Boost Enhances the Antitumor Immune Response Elicited by Plant-Virus-Based Cancer Vaccine. *J. Am. Chem. Soc.* **2019**, *141*, 6509−6518.
(80) Shukla, S.; Jandzinski, M.; Wang, C.; Gong, X.; Bonk, K. W.; Keri, R. A.; Steinmetz, N. F. A Viral Nanoparticle Cancer Vaccine Delays Tumor Progression and Prolongs Survival in a HER2 + Tumor Mouse Model. *Adv. Ther.* **2019**, *2*, 1800139.
(81) Smith, A.; Perelman, M.; Hinchcliffe, M. Chitosan. *Hum. Vaccines Immunother.* **2014**, *10*, 797−807.
(82) Mohsen, M. O.; Augusto, G.; Bachmann, M. F. The 3Ds in Virus-like Particle Based-Vaccines: "Design, Delivery and Dynamics. *Immunol. Rev.* **2020**, *296*, 155−168.
(83) Zellweger, R. M.; Wartel, T. A.; Marks, F.; Song, M.; Kim, J. H. Vaccination against SARS-CoV-2 and disease enhancement - knowns and unknowns. *Expert Rev. Vaccines* **2020**, *19*, 691−698.
(84) Munoz, F. M.; Cramer, J. P.; Dekker, C. L.; Dudley, M. Z.; Graham, B. S.; Gurwith, M.; Law, B.; Perlman, S.; Polack, F. P.; Spergel, J. M.; Van Braeckel, E.; Ward, B. J.; Didierlaurent, A. M.; Lambert, P. H. Vaccine-associated enhanced disease: Case definition and guidelines for data collection, analysis, and presentation of immunization safety data. *Vaccine* **2021**, *39*, 3053−3066.
(85) Lee, W. S.; Wheatley, A. K.; Kent, S. J.; DeKosky, B. J. Antibody-Dependent Enhancement and SARS-CoV-2 Vaccines and Therapies. *Nat. Microbiol.* **2020**, *5*, 1185−1191.
(86) Hotez, P. J.; Corry, D. B.; Bottazzi, M. E. COVID-19 Vaccine Design: The Janus Face of Immune Enhancement. *Nat. Rev. Immunol.* **2020**, *20*, 347−348.

https://doi.org/10.1021/acs.biomac.2c00112
Biomacromolecules 2022, 23, 1812−1825